TECHNICAL MEMORANDUM

329

The impact of new sub-grid scale orography fields on the ECMWF model

U. Uhrner

Research Department

January 2001

European Centre for Medium-Range Weather Forecasts
Europäisches Zentrum für mittelfristige Wettervorhersage
Centre européen pour les prévisions météorologiques à moyen

1 Introduction

Increased resolution of numerical weather prediction models resolves finer scale motions and provides a more accurate description of the effects of topography. As a consequence higher resolution input data is needed for orography and the sub-grid scale orography (SGO) fields used for the computation of gravity-wave-drag and blocked flow drag.

The model that was operational in 1998 used SGO fields derived from the US-Navy terrain elevation data set with a resolution of 10 arcmin (about 20 km). Because of the coarse resolution and serious regional errors (especially over Antarctica) the mean height was replaced in March 1998 by merged DTM5 (about 5 km) and GLOBE (1 km) data on a nominal resolution of 2'30". The SGO fields were not replaced at the time because the new fine scale orographic data changes them substantially, which requires extensive testing. In particular the slope increases with higher resolution.

New SGO fields for standard deviation μ, slope σ, orientation θ and anisotropy γ used in the SGO parametrization scheme, as well as mean height were computed from recently available global GTOPO30 terrain height data spaced at 30 arcseconds (about 1 km) for various target resolutions. For the area of Greenland GTOPO30 data were replaced by KMS Greenland DEM data because of their higher accuracy.

Variance spectra and spectra representing the slope parameter were calculated for different mountainous areas. For small areas, the 30 arcsecond spectra are compared with those from 3 arcsecond data (about 70 m) to study the contributions beyond the scale of the 30" data.

The software to process the climate fields has been adapted for the new 30" orographic data. First the data is averaged to an intermediate resolution of 2'30", and then the SGO fields are computed from the 2'30" data after subtracting the linearly interpolated mean orography at target resolution (in the old software the subgrid fields were computed with respect to the stepwise changing orography on the target grid). The choice to use horizontal scales between target resolution and 2'30" only for the SGO fields was recommended by ECMWF Workshop on orography in 1997 because gravity waves with shorter horizontal wave length do not propagate in the vertical. Later the scales smaller than 2'30" will be used for the roughness length parametrization.

Due to these changes, most of the new sub-grid scale orography fields for the SGO scheme have changed substantially. The field for slope σ has increased globally by a factor of 1.7 and over mountain ranges by a factor of 3 to 4. Consequently the surface drag produced by the SGO scheme in the model is changed significantly because it depends linearly on the slope.

The impact of the new fields on winter and summer model climate is evaluated and some winter climate runs with changed drag constants were carried out aiming to adjust the scheme to the new fields as much as possible. In addition extensive testing of medium range forecasts was

carried out.

2 New SGO fields and code changes

2.1 The ECMWF sub-grid scale orography scheme

The SGO scheme is described in detail by *Lott and Miller (1997)*; only a brief description will be given here. Sub-grid scale orographic effects following *Baines and Palmer (1990)* are combined with ideas of bluff body dynamics to represent non linear mountain drag. The orography as described by the GTOPO30 (*Gesch and Larson 1998*) and Greenland KMS DEM (*Ekholm 1996*) on 30" is converted into i) a mean orography and ii) SGO fields representing height variations with respect to the resolved mean elevation, characterized by standard deviation μ, slope σ, orientation θ and anisotropy γ.

The flow types are in principle separated into two main classes according to whether $2NH/U$ is less or greater than unity. N is the Brunt-Väisälä frequency, U is the wind speed of the incident flow, and H is the height of the mountain tops. The scheme treats explicitly low level flow blocking when the effective height of the model mountain is sufficiently high. This drag is parametrized on model levels which are intersected by SGO fields. Drag is computed by combining formulae valid for elliptical mountains with real orographic data. In the parametrized form, the flow below the blocking height Z_b separates at the mountain flanks and goes around generating blocked flow drag, whereas the upper part of the low level flow goes over the topography and generates gravity waves. Z_b is the highest level below the mountain tops for which

$$\int_{Z_b}^{3\mu} \frac{N}{U_p} dz \geq H_{nc} \ ,$$

where U_p is the wind speed in the direction of the incident flow and H_{nc} is a critical value set to 0.5. After some assumptions and simplifications the blocked-flow drag is calculated in the following way:

$$\begin{aligned} \mathbf{D}_b(z) &= -C_d max(2-\frac{1}{r},0)\rho\frac{\sigma}{2\mu}\left(\frac{Z_b-z}{z+\mu}\right)^{1/2}(Bcos^2\psi+Csin^2\psi)\frac{\mathbf{U}|\mathbf{U}|}{2} \ , \\ with \quad r &= \frac{cos^2\psi+\gamma sin^2\psi}{\gamma cos^2\psi+sin^2\psi} \ . \end{aligned}$$

Hereby the eccentricity of the obstacles, the directionality of the flow to the main ridge and the width of the obstacle as seen by the flow are considered in the parametrization. This

equation is applied below Z_b to the horizontal momentum equations. Parameter ψ is the angle between the geographical orientation of the sub-grid scale orography θ (the orientation of ridges relative to East) and the wind direction φ. C_d is the drag coefficient for the blocked flow which is modulated by the aspect ratio of the obstacle, to account for the anisotropy of the obstacle. The constants $B(\gamma)$ and $C(\gamma)$ are the *Phillips (1984)* parameters and defined as $B = 1 - 0.18\gamma - 0.04\gamma^2$; $C = 0.48\gamma + 0.3\gamma^2$ (γ is anisotropy). They describe the pressure perturbation due to the elliptical shape of mountains.

The gravity wave part of the scheme is based on the work by *Miller et al.(1989)* and *Baines and Palmer (1990)*, and takes into account three dimensional effects in the wave stress amplitude and orientation. The equation used to calculate the mountain wave stress is similar to that proposed by *Phillips (1984)* with the assumption that the sub-grid scale orography consists of elliptically shaped mountains:

$$(\tau_1, \tau_2) = \rho_H U_H N_H \mu\sigma G\{Bcos^2\psi_H + Csin^2\psi_H, (B - C)sin\psi_H cos\psi_H\}.$$

The basic parameters ρ_H, U_H and N_H are evaluated as averages over the layers between μ and 2μ above the model's lower boundary which is the mean orography. The vertical distribution of the gravity wave stress will determine the levels at which the waves break and slow down the synoptic flow. The breaking of waves occurs when the total Richardson number Ri falls below the critical value Ri_c. When low level breaking occurs in the scheme, the drag is distributed above the blocked flow over a layer with a thickness equal to a quarter of the vertical wavelength of the waves. Above this layer, the stress remains constant when $Ri > Ri_c$ until Ri falls below the critical value of Ri_c.

The scheme depends essentially on the five parameters, G, Ri_c, H_{nc}, C_d for the blocked flow and C_d for the upper level drag which could be changed to accommodate for the changed sub-grid scale orography fields. G is a function of mountain sharpness. The operational values are: $C_d = 1.0$ (GKWAKE) for the lower levels, $C_d = 0.3$ (GKDRAG) for the upper levels, $G = 1$, $Ri_c = 0.25$ and $H_{nc} = 0.5$.

The specification of sub-grid scale fields is described in detail by *Lott and Miller (1997)*;

2.2 New sub-grid scale orography fields

2.2.1 Terrain height data sets

GTOPO30 is a global digital elevation model (DEM) with a horizontal grid spacing of 30 arcseconds. Detailed information on the characteristics of GTOPO30, including production methods and accuracy, is found in *Gesch and Larson (1998)*. GTOPO30 data were downloaded (free of charge) from the Internet. The data of the Greenland Ice Sheet were obtained from Kort-og Matrikelstyrelsen (National Survey and Cadastre, Denmark), for detailed information

see *Ekholm (1996)*. The difference between GTOPO30 and USNAVY derived SGO fields will be described here briefly.

2.2.2 Changes in the processing software for sub-grid scale orography fields

Following the recommendations of the *ECMWF Workshop proceedings on orography 1997*, all sub-grid scale quantities related to the SGO parametrization are computed from the scales representing the physics of the forcing mechanisms, e.g. of order 5 km for trapped lee waves which corresponds approximately to 2'30". First, an area averaged mean height was computed from 30" data at 2'30" resolution, then fields for standard deviation, slope, anisotropy and orientation were calculated for various target grids. To avoid "double counting" the resolved scales were filtered out. In the old operational version, the zonal derivatives $\partial h/\partial x$ are computed as central differences in arc space. This was corrected because of the poleward convergence of the meridians and the resolution dependence of σ, θ and γ.

The code changes in the processing software were only applied to the new terrain elevation data. Hereafter the result of changing the processing software and computing new sub-grid scale fields from new data will be referred to as "**new fields**".

2.2.3 Brief description of changes in the new sub-grid scale fields

Table 1: Global means for height, standard deviation, slope, orientation and anisotropy, computed from US-Navy (except the averaged height which is from DTM5 and GLOBE data) and GTOPO30 data.

	avh	stddev	slope	orient	aniso
US-Navy	231.6 m	36.45 m	0.002241	0.5466	0.0947
GTOPO30	232.0 m	34.73 m	0.003854	0.4997	0.1521

In particular sub-grid scale fields for slope, anisotropy and orientation which are calculated from derivatives of the terrain height changed significantly. Near most mountain ranges lower values have been obtained for μ which is caused by filtering out the resolved standard deviation. The slope parameter σ is in most of the mountainous areas significantly increased. Slope decreased only in the polar regions because of equal area derivatives and less variable structure of ice-shields where the resolved slope was filtered out. Anisotropy and orientation from 30" data look substantially different from the US-Navy derived fields. Both fields show an enormous variability. Sub-grid scale parameters for a given area on target resolution (e.g. T319) can be displayed on scatter plots, where the x-axis corresponds to GTOPO30 values and the y-axis to US-Navy values. Linear regression analysis shows that σ increases over principal mountain ridges by a factor of 3 to 4. A general feature of higher resolution terrain data is that μ and

especially σ are increased close to the main ridges, and that near foothills μ and σ are often reduced. Table 1 and table 2 provide some statistics about the new fields. The scatter plot of figure 1 shows the new slope parameters versus the old one for the Alps.

Table 2: Regression analysis of US-Navy slope (y) against GTOPO30 slope (x) for mountainous areas. The equation for the linear fit and the correlation coefficient are given.

Norway	Alps	Andes	Himalayas
$y = 0.31x + 3.7 \cdot 10^{-3}$	$y = 0.23x + 8.9 \cdot 10^{-3}$	$y = 0.29x + 1.3 \cdot 10^{-2}$	$y = 0.25 + 8.9 \cdot 10^{-3}$
0.67	0.67	0.48	0.59

Zonal averages of SGO fields μ, σ and γ at T63 resolution are shown in figure 2. The new field for the mean height is virtually identical; the standard deviation (μ) is slightly lower at most latitudes. The new slope (σ) is about a factor of two higher from about 70°N to 50°S, but lower over the Antarctic continent. For anisotropy γ we obtain a non uniform picture; in general the new field is more isotropic especially between 80°N - 50°N and 75°S - 90°S. Considering the changes to the SGO fields we can expect that the increased slope will increase the drag from the SGO scheme and reduce the zonal mean flow.

2.3 Code changes in the IFS

Bugfixes

During the work on the SGO fields, two bugs in the formulation of the SGO scheme were discovered by B. Ritter at DWD:

- The basic parameters ρ_H, U_H and N_H were evaluated between the model's lower boundary and 2μ and not as described by Lott and Miller *(1997)* between μ and 2μ.
- The critical level and subsequent gravity wave breaking could occur at levels lower than μ, which was unintentional.

Drag constants

To compensate for changed sub-grid scale fields, different values for lower level (GKWAKE) and upper level drag constant (GKDRAG) were tested. In the old scheme GKWAKE is set to 1.0 and GKDRAG is set to 0.3. Sensitivity experiments were carried out by changing these parameters (see Table 4).

2.4 Spectral terrain representation

Different studies show that SGO fields depend on the resolution of the source data. *Mengesha (1997)* pointed out that there has been no convergence for the slope parameter (as used in the ECMWF SGO scheme) for the studied area of the Sand Hills (Newbraska). The silhouette area A of the roughness elements in the horizontal area S or silhouette slope (A/S) is also strongly dependent on the resolution of the orography used *(Taylor 1997)*. Variance spectra for terrain height can give information about the scales which need to be resolved in a model or need to be parametrized. *Young and Pielke (1983)* studied terrain height variance distributions for three areas in the Rocky Mountains near Denver in order to determine the required horizontal grid spacing for mesoscale models. They concluded that 0.1 km is a likely maximum allowable value of horizontal grid spacing to neglect sub-grid scale parametrization for the jagged terrain of the investigated areas. The exponent of the power law fit to terrain height variance spectra provides a quantitative measure of the appearance of terrain "smoothness". The exponent increases (variance against wavenumber) with increased jaggedness of the terrain at short wave lengths *(Young and Pielke 1983)*. Results of previous studies vary in a range of k^{-1} to k^{-4} depending on the wavelength band, the areas studied and the representation, where k denotes the wavenumber (see Table 3). In addition, variance spectra for terrain height can give some information about the roughness of individual mountain ranges and can be used for parametrization of gravity waves *(Bannon and Yuhas 1990)*.

Table 3: Overview of published power law spectra with k representing wave number except for Mengesha (1990), where k is zonal wave number and m is meridional wave number.

Author	Area	Resolution	Wavelength band	Exponent power law fit
Bannon and Yuhas (1990)	Appalachian Mtns (Pensylvania)	0.7 km	1.4 - 358 km	$k^{-1.72}$
Bretherton (1990)	Wales	5 km	10 - 90 km	$k^{-1.5}$
Mengesha (1997)	Sand Hills (Newbraska)	0.05 km	0.1 km - 25 km	$k^{-2.3}$, $m^{-2.8}$ (for high k)
Smith and Gleason (1997)	West Coast to) Cont. Divide (USA)	0.07 km	0.014 - 1080 km	k^{-2} - k^{-4}
Young and Pielke (1983)	Appalachian Mtns Virginia	0.76 km	0.14 - 100 km	$k^{-1.66}$ - $k^{-2.25}$
	Rocky Mtns: Boulder (Col)	0.7 km	0.14 - 85 km	k^{-1}
	South Park (Col)	0.7 km	0.14 - 428 km	$k^{-0.96}$

Several authors found different spectral slopes for the same area which presumably indicate that different geomorphical processes are acting. This is not consistent with a fractal interpretation of the spectrum as *Gilbert (1989)* pointed out. *Mark and Arondson (1984)* found for many

areas two scale breaks at around 1 km and around 5 km. *Steyn and Ayotte (1985)* showed with two-dimensional terrain height spectra for 60 m resolution data that the spectral roll-off is strongly dependent on direction.

One-dimensional terrain height variance spectra were computed to characterize the terrain at the scales considered in the SGO parametrization, to characterize smaller scales and to validate the data. The smaller scales are of particular interest for the slope parameter which is crucial for the aerodynamic roughness length. Therefore terrain elevation data available for areas for the U.S. spaced on 3 arcseconds were also processed. Depending on the resolution of the data, the power spectral densities were computed for multiple cross sections using a FFT algorithm within adjacent 1 degree blocks. For each wavenumber along x, all spectra were averaged over y to give a 1-d representation of the power spectrum. For each cross section, a linear trend was first calculated and then subtracted from the terrain height series. The spectral energy density multiplied by the squared wavenumber represents the spectrum of the slope parameter. Some North-South spectra were also computed to evaluate the effect of directionality.

Digital topographic data spaced on 3 arcseconds were obtained from USGS. The quoted vertical accuracy for this data is +/- 30 m (linear error at 90% probability). The data sources are the same as used for GTOPO30.

All the variance spectra computed from 30" data for different mountainous regions of the world showed roughly two different spectral slopes with a transition zone between $0.1 < k < 1$ which corresponds to wavelengths between 50 km and 5 km (see figure 3). The chosen Andes cross-section shows the steepest spectral slope before ($k^{-1.8}$) and after the scale break (up to k^{-4}). The tail at the end of the spectra may be attributed to an aliasing problem caused by sampling strategy in the source data. Also the Karakorum shows a steeper spectral slope for the smaller wave numbers and k^{-3} for the higher wave number range. The spectral slope for Tibet is the lowest in the small wave number area. The Alps and Norwegian mountains are in between. The spectrum for the cross-section from the US West coast to the Continental divide gives in the lower wave number range an uneven picture maybe due to the fact that different mountain ranges are within the section. The area of the Black Forest and Vosges looks quite different from the other regions, the spectra show no scale break and have the lowest slope at the end of the spectra. However there is no noteworthy ragged terrain. Also the spectra for the SW of USA show a low spectral slope for $k > 1$. The results are in contradiction to *Young and Pielke (1983)* and suggest that the intercept is of equal importance because the variance is a better measure for the jaggedness of the terrain.

The West-East spectra representing slope show a maximum near the range of the scale break (see figure 3). The main contributions for slope are in the range of the scale separation for the cross-sections of the Alps, S-Norway, the Karakorum and also Tibet. It looks as if there is another scale break around k = 5.

The variance spectra from 30" and 3" data are identical for areas in the USA. Spectra from 3" indicate a stronger directionality at small scales (only one example is shown, see figure 4). The

variance spectra for the cited regions could be reproduced fairly well except for the the Rocky Mountains near Denver (see figure 3 and figure 4). A spectral slope of about 1.8 for North-South and 2.1 for West-East was obtained for the larger wavenumbers, and about 3 for North-South and 3.5 for West-East for the small wavenumbers (not shown). For Wales a spectral slope of $k^{-1.8}$ was obtained, which is different from *Bretherton*'s results, but he used data sampled every km from topographic maps. The difference in spectral slope between smooth appearing possibly older mountain ranges and ragged younger mountain ranges is not so clear as pointed out by *Young and Pielke (1983)*. However, the total terrain height variance seems to be significantly higher for ragged mountain ranges. The terrain height variance spectra converge for all spectra for the higher wavenumbers. Even if we do not believe the tail of the slope spectra, there is no convergence for slope (see figure 4). For convergence the exponent of the power law must be smaller than -3 for slope and smaller than -1 for the variance.

From the spectra it can be concluded that cut-off at 5 *km* for the SGO fields is highly relevant and is in fact a parametrization choice. At scales smaller than 5 *km* there are still significant contributions to variance and slope. These small scales are excluded as input to the SGO parametrization and left to the orographic roughness length parametrization.

3 Impact on model climate

3.1 Description of experiments

The impact on northern hemispheric winter and summer climate was studied with 6 member ensembles of 120-day integrations. The operational SST fields were used as time dependent lower boundary condition. The studied quantities were averaged over the last 3 months and over the 6 members of the ensemble.

Experiments were carried out with the new and old SGO fields, with adjusted parameter settings, and for reference, also with the SGO scheme switched off. For the winter climate runs DJF 1996/97 was chosen and for summer climate JJA 1996. Concerning the significantly changed slope field, experiments with changed drag constants were carried out in order to adapt as much as possible the SGO scheme to the new data. To evaluate the impact of the two bugs in the SGO-scheme a few more calibration experiments were carried out. In addition further experiments with 50 and 31 level for DJF 98/99 were run to see if the results obtained with 31 level also hold for increased vertical resolution and for a different winter season. Table 4 gives an overview of the different experiments.

Table 4: Overview of experiments at T63 31 levels with model cycle CY18R6

experiment	sgs fields	season	GKWAKE	GKDRAG	remarks
zv5h	old	DJF 96/97	1.0	0.3	control experiment
zvzo	old	DJF 96/97	0	0.3	
zvpj	old	DJF 96/97	0	0	
zwlc	old	DJF 96/97	1.0	0.3	bugfix I+II
zw9k	old	JJA 96	1.0	0.3	control experiment
zw9m	old	JJA 96	0	0	
zwu2	old	JJA 96	1.0	0.3	bugfix I+II
zy5t	old	DJF 98/99	1.0	0.3	bugfix I+II
zy1g	old	DJF 98/99	1.0	0.3	bugfix I+II 50 level
zv8w	new	DJF 96/97	1.0	0.3	new sgs only
zvod	new	DJF 96/97	0	0.3	
zvo4	new	DJF 96/97	1.0	0	
zvo9	new	DJF 96/97	0	0	
zw1m	new	DJF 96/97	0.33	0.3	
zw5i	new	DJF 96/97	0.33	0.2	
zw5s	new	DJF 96/97	0.33	0.9	
zwau	new	DJF 96/97	1.0	0.3	bugfix I
zwiu	new	DJF 96/97	1.0	0.3	bugfix I+II
zwcl	new	DJF 96/97	0.2	0.4	bugfix I+II
zwu0	new	DJF 96/97	1.0	0.2	bugfix I+II
zwwt	new	DJF 96/97	0.5	0.3	bugfix I+II
zx3j	new	DJF 96/97	1.0	0.27	bugfix I+II
zw9l	new	JJA 96	1.0	0.3	
zw9n	new	JJA 96	0	0	
zwu1	new	JJA 96	1.0	0.3	bugfix I+II
zy5s	new	DJF 98/99	1.0	0.3	bugfix I+II
zy1f	new	DJF 98/99	1.0	0.3	bugfix I+II 50 level

3.2 Evaluation

For all experiments the geopotential height at 200 hPa, 500 hPa and 1000 hPa was plotted as well as cross-sections for differences with the analysis of zonal mean wind and zonal mean temperature. Cross-sections of the root mean square error of the differences to the analysis were computed to get some information about how well longitudinal variations of the zonal mean flow and the zonal mean temperature are captured. For the control experiments with corrected bugs the meridional heat flux and eddy momentum flux were calculated and the impact on the

general circulation was assessed. Many experiments have been carried out and only the most important features will be discussed.

3.2.1 The impact of the SGO scheme for DJF 1996/1997

The effect of the SGO scheme on zonal mean flow and temperature is demonstrated by the comparison of the control integration (zv5h) with an integration without SGO scheme (experiment zvpj, old SGO fields). The strength of the zonal mean flow is clearly reduced with the SGO scheme at all levels between 40°N - 60°N (see figure 5 and 6). The jet structure is improved with a stronger subtropical jet and a weaker polar night jet. In the tropics and Southern Hemisphere there are only minor changes (not shown).

The zonal mean temperature distribution shows a cold bias in the integration without SGO scheme. With sub-grid scale drag the changed zonal wind distribution modifies the temperature distribution by induced mean meridional circulations in order to maintain the constraint of the thermal wind balance (see figure 7). The Ferrel cell circulation is weakened by the sub-grid scale drag (not shown). As shown by *Palmer et al. (1986)* a substantial adiabatic warming north of the drag maximum occurs accompanying the overall decrease in zonal wind. Figure 8 shows some improvement in MSLP over the North Atlantic, Europe and the North Pacific with sub-grid scale drag, however the shape of pressure distribution with drag is not represented in a satisfying way. The Islandic low is too deep, and the Baltic Low is not resolved. Instead of a shallow anticyclone over the Balkan there is a prominent anticyclone over the southwestern diterranean simulated. The Aleutian Low is too far west, as in the simulation without g. The Siberian high, which is too low without drag, is simulated far to strong with drag. At 500 hPa a quite similar picture is obtained. The Southern Hemisphere shows almost no sensitivity to the sub-grid scale scheme.

3.2.2 The impact of the new SGO fields for DJF 1996/1997

As can be seen from figure 9, the new SGO fields give improvements to the zonal mean flow in both hemispheres. Over large areas, the differences to the analysis are reduced by 1-2 m/s and the mean flow is clearly improved between 40°N - 60°N. However in the region above the northern subtropical jet where the flow is already too weak in the control, the reduction is too large. In contrast, over the polar lower stratosphere the flow is about 1-2 m/s too strong. With the new fields the magnitude of the southern subtropical jet is well reproduced and the latitudinal displacement of the subtropical jet, which is the main problem there, is also improved. However the errors still remain large between 20°S - 70°S. This misplacement might result from temperature errors in the planetary boundary layer. Around the Antarctic continent a cold bias (up to 4K, not shown) exists, whereas the Antarctic continent shows a warm bias together with a geopotential height bias at 500 hPa of up to 8 dam.

Peak warm biases of about 3-4 K occur at 200 to 100 hPa near 60°N (figure 10). Although the forcing of the gravity wave stress is enlarged by a factor of about two compared to the control, the warming effect north of 40°N is clearly less than in the control experiment compared to the no drag experiment. Consequently the zonal mean temperature deteriorates slightly over the polar Northern Hemisphere. In comparison to the control experiment the Ferrel cell circulation is slightly weaker with the new fields in the Northern Hemisphere (not shown).

The area of the main deceleration of the zonal mean flow coincides with the latitudes of the major increase in slope for the Northern Hemisphere (see figures 2 and 9).

At 500 hPa the errors are in total larger with the new sub-grid scale fields for the Northern Hemisphere but lower for the Southern Hemisphere (see figures 11 and 12). The general flow pattern looks improved over Europe, and the Southern Hemisphere but not for the Pacific Ocean. Over Europe the ridge and the diffluent flow is better reproduced than in the control experiment. The Antartic vortex is 2-6 dam too high against up to 10 dam in the control. Between 30°S and 60°S the errors are over large areas reduced by 2 dam. However there are still huge differences to the analysis because the structure of the simulated flow is in general too zonal. Over land and close to the continents the errors become clearly smaller.

At 200 hPa the errors look similar to 500 hPa, in principle for most areas the errors are just enforced. For the Northern Hemisphere the impact is neutral and for the Southern Hemisphere there is some improvement. Also for 1000 hPa or MSLP the errors are located in almost the same areas. This is a general feature of these experiments, the errors look very barotropic (see figures 13 and 14).

3.2.3 Impact of bugfixes for DJF 1996/1997

The bugfixes were tried with the old SGO fields and the new ones. In the configuration with the new SGO fields, the comparison of the standard model version (zv8w), the version with bugfix I (zwau), and the version with bugfix I+II (zwiu) showed that there is only little sensitivity to bugfix II and some impact due to bugfix I (see section 2.3 for a description of the bugfixes).

For the zonal mean flow, the impact is generally neutral, but the zonal mean temperature is slighly improved compared to the model with the uncorrected code (experiment zwiu versus zv8w both using the new SGO fields). However, the geopotential height at 200 hPa, 500 hPa, 1000 hPa improves over large areas in the Northern Hemisphere (for the 500 hPa height see figures 11, 15). The impact on height and wind field is neutral for the Southern Hemisphere. Also the wind field at 200 hPa is better represented with both bugfixes. For the Southern Hemisphere the impact of the bugfixes was neutral.

In contrast, the bug corrected set of integrations with operational fields (zwlc) was slightly outperformed by the control (zv5h), the geopotential height deteriorates in some areas by about

+/- 2 dam. The zonal mean flow and temperature distributions remained nearly unchanged.

In conclusion, the bugfixes showed some impact on DJF integrations, but the effect is smaller than the impact of new sub-grid scale fields.

3.2.4 Impact of new fields with corrected SGO code

To see whether the impact of the new fields is altered by the bugfixes in the SGO scheme, the experiments of section 3.2.3 were repeated with the corrected code.

This comparison clearly shows a beneficial impact of the new fields. Zonal mean wind is significantly improved in both hemispheres, and the mean geopotential height at 500 and 200 hPa are improved in both hemispheres (see figures 15 and 16).

Figure 18 shows the Northern Hemisphere wind field at 200 hPa. With the new fields the flow over the North Atlantic and Europe as well as in the North Pacific is improved.

Figure 19 and figure 20 show the zonal mean distribution of the meridional and zonal stresses from the SGO scheme. The meridional component is for both experiments clearly lower than the latitudinal but significantly enlarged with the new fields. Between 30°N and 50°N the zonal stress for the upper levels is about a factor of two larger; for the polar areas the stresses are smaller. Between 40°S and 50°S there is a notable increase also at the upper levels (see figure 21 for the averaged tendencies of zonal wind due to the SGO scheme). The upper level drag acts very localized on the upper level flow. The peak deceleration rates are near 30°N in the lower stratosphere. With the new fields, less gravity wave breaking occurs at the model top between 30°N and 70°N. Also the drag distribution at the 6 lowest model levels is strongly affected by the new SGO fields.

The results show that stronger wave drag in the Northern Hemisphere decelerates the mean westerlies in the troposphere and the adjustment to thermal wind balance warms the polar stratosphere by adiabatic descent. The pressure gradient force is over large mid latitude areas lowered (see figure 15) and the mean meridional circulation is slightly weakened (not shown) in the Northern Hemisphere. In the global angular momentum budget the balance of large scale mountain torques by reduced zonal flows is obtained by reduced eddy flux convergence in the Northern Hemisphere (see figure 22). The reduction of momentum fluxes is an improvement (see figure 24). In the Southern Hemisphere the position of the mid latitude momentum flux is improved, but the magnitude deteriorates. The heat flux is improved in the Northern Hemisphere in particular in the polar stratosphere (figure 23). The tropospheric heat flux is slightly worse in the Southern Hemisphere. Again there is the usual misplacement of about 5 degrees.

In summary, the introduction of the new SGO fields results in a systematic improvement of the model climate. The bugfixes have only marginal impact and do not change the sensitivity to

the new fields.

3.2.5 Impact of modified drag constants for DJF 1996/1997

Before the bugfixes were introduced, some experiments with changed drag constants were already conducted. The aim was to find the optimum ratio between upper and lower level drag. First two experiments without lower level drag were run, with the operational fields (zvzo) and the new fields (zvod). The integration for the new fields with omitted low level drag showed some interesting results. The zonal mean flow was improved in both hemispheres at the cost of the temperature distribution. At 60°N 200 hPa a warm bias was obtained. At 500 hPa and 1000 hPa the height differences to the analysis are smaller than in the control integration. Nevertheless the shape was not very well represented. The flow appears too zonal, distinct subtle patterns are missing. The corresponding integration with the operational fields shows only small changes compared with the control.

In addition an integration without upper level drag was run (zvo4) which showed clearly worse results, similar to the experiments with deactivated SGO scheme.

Since the experiment with omitted low level drag (zvod) gave surprisingly good results (not shown), the lower drag constant was kept at one third of the operational value and the drag constant for the upper part was varied in the following way: i) lowered for experiment zw5i, ii) kept the same for experiment zw1m, and iii) enhanced by a factor of three for zw5s. The latter simulates the increase in subgrid slope that would be obtained by not cutting off the spectrum at 2'30" but by keeping all the information down to 30" resolution. *(personal communication B. Ritter).* The results are:
i) For the low drag case (zw5i), small differences have been obtained at 500 hPa and 1000 hPa (of the same magnitude as with the bugfixes). The zonal mean flow was only slightly changed. The zonal mean temperature is about 1 - 1.5 K warmer above 300 hPa between 50°and 90° N.
ii) Similar results have been obtained with the higher level constant kept (zw1m) compared to the integration with new fields only (zv8w). All in all, zw1m was worse than zv8w and there was no improvement compared to zv5h.
iii) The high drag experiment was clearly slowing down the zonal flow too much in the Northern Hemisphere, in particular above 200 hPa. In the Southern Hemisphere the typical dipole error structure was shifted about 3 °northward but the errors remain. Above 350 hPa, the temperature has been increased up to 8° K and below decreased by up to 2° K. At 200 hPa, 500 hPa and 1000 hPa the errors are (together with the experiment zwau) lowest for the N-Pacific area.

Figure 25 shows the sensitivity of higher and lower level meridional and latitudinal stresses for the experiments with changed drag constants and the control with new SGO fields. The upper level stress is sensitive to changes in the lower level stress as figure 25 shows. When the low level drag constant is chosen smaller (by a factor 3 in zw1m compared to zv8w) the upper level

drag is enhanced and the low level drag is decreased, but the decrease is less than a factor 3. The lower level stress is less sensitive to changes in the upper drag constant.

For the calibration experiments with bugfixes the experiment zwiu was chosen as a reference and the drag constants were changed. With 80% less low level drag and 30% more high level drag (zwcl) only worse results have been obtained. Also 30% reduced upper level drag have not been beneficial for the results. No benefit has been gained with halved lower level drag constant (zwwt), too. However 10% reduced upper drag (zx3j) has been able to outperform zwiu. The zonal mean flow is improved in the polar stratosphere and also the warming is reduced.

3.2.6 JJA 1996 experiments

The impact of the bugfixes was neutral. Therefore, the impact of the new SGO fields will be discussed from the simulations with bugfixes only (comparing zwu2 and zwu1).

The zonal mean flow shows some improvement in the higher troposphere and lower stratosphere which alleviates the too strong westerlies by 1 - 4 m/s in the Southern Hemisphere. The south polar stratosphere is warmed up but less than the north polar stratosphere in the DJF run. The northern hemispheric zonal flow and temperature are hardly affected. The difference to the analysis indicates a similar latitudinal misplacement of the subtropical jet for the north summer as shown before (DJF 1996/97) for the Southern Hemisphere summer.

At 500 hPa there is not much difference between the two experiments in the Northern Hemisphere as well as for the Southern Hemisphere. The experiments are not able to reproduce the subtle troughs and ridges shown in the analysis over the Southern Hemisphere. At 200 hPa, the experiment with the new fields shows more skill, similar to the wind at 200hPa over the Northern Hemisphere (no figures are shown).

3.2.7 DJF 1998/99 31 level experiments

The motivation to run these experiments was twofold: firstly to see how the previously obtained results compare with other winter climate seasons, and secondly to compare the results with 50 level experiments. With the new fields (zy5s) the zonal mean flow is improved in the Southern Hemisphere. In the Northern Hemisphere the tropospheric mean flow is improved between 40°-70°N, but the westerlies at 100 hPa are slowed down too much. It appears that this season is less sensitive to changes in the SGO for the Northern Hemisphere (figure 26), because there are smaller differences in the zonal mean flow compared to the DJF 96/97 period (experiment zwiu and zwlc).

Again, warming of the polar lower stratosphere and higher troposphere is involved, which, in this case is less detrimental compared to the analysis (figure 27). At 500 hPa, a similar picture

to DJF 1996/97 is obtained; over the N-Atlantic and Europe the flow is improved, but the trough east of the Asian continent is not prominent enough and misplaced. The Southern Hemisphere is improved at 500 hPa and 200 hPa (not shown).
Altogether, the impact of the new fields for DJF 1998/98 is neutral for the Northern Hemisphere and positive for the Southern Hemisphere.

3.2.8 DJF 1998/99 50 level experiments

For the DJF 1998/99 period the results for 50 vertical model levels resemble the experiments on 31 levels. The impact of the new fields is positive for the Southern Hemisphere and neutral in the Northern Hemisphere. With higher vertical resolution the warming is increased at the lower polar stratosphere. Also the errors are slightly increased for both fields with higher resolution. At pressure levels 200 hPa and 500 hPa the differences to the analysis are similar to the 31 level integrations.

4 10-day forecast experiments

Apart from studies of impact in longer integrations a number of ten-day forecast experiments were run to examine some instantaneous fields and the impact on forecast performance. The drag constants remained in all experiments unchanged.

To illustrate the impact of the new fields, some fields were plotted for the first 24 hours for a set of 2 forecasts at T319 resolution with 31 vertical levels. The distribution of gravity wave stress is clearly enhanced with the new fields (zwzm) in mountainous regions in between 60°N - 60°S. In polar regions the stresses are reduced. Consequently the dissipation is also increased at mid latitudes and slightly decreased in polar regions.

The impact on the boundary layer scheme is small. The boundary layer surface stress is slightly reduced, as well as the boundary layer dissipation (global mean about 2%). The mean sea level pressure distribution changes, the lows are filled, and anticyclones have lower pressure.

Two sets of 24 ten-day forecast only experiments with initial dates on the 1st and 15th of each month were carried out for July 1997 until June 1998. Figure 30 shows anomaly correlation of height errors for 500 hPa. In general the impact is neutral for both hemispheres, for the area of North America the scores are slightly better, for Europe slightly worse.

The bugfixes showed no impact on the scores of the December period. The run with the new sub-grid scale fields and the bugfixes improved the scores for North America, whereas in other regions they remain neutral.

The 60-level configuration with new SGO fields, performed well compared to the 60-level configuration with old fields for a series of 21 ten-day forecasts for January 1999. The scores were better or neutral for all areas. Especially over E-Asia and the N-Pacific was quite some improvement (figure 30). Also a 22 day long summer period, starting at August 20 showed a very positive signal over E-Asia. The scores also improved over the N-Atlantic and Europe. In general both forecast series show for the Northern Hemisphere improved scores and for the Southern Hemisphere a neutral result.

5 Conclusions and outlook

The influence of significantly changed new SGO fields and a revised processing software were extensively tested with winter and summer climate integrations as well as 10 day forecast experiments. Furthermore an attempt was made to optimize the parameterization constants in the SGO scheme in conjunction with the new fields.

The major changes in sub-grid scale fields result in a nearly doubled SGO drag and generally in a positive impact on the model climate. The positive impact was not confined to winter climate.

The positive results were obtained without further optimization of the parametrization constants. The fields for geopotential, zonal mean flow and zonal mean temperature showed less sensitivity to these parameters than expected. It appears that with the new fields, the scheme shows some beneficial sensitivity in the Southern Hemisphere. In particular the zonal mean flow improved. The zonal mean temperature is slightly deteriorated at the lower arctic stratosphere. The best results for DJF 1996/97 runs were obtained with a 10% reduced upper level drag constant.

The results for the 50 level DJF simulations did not confirm this and showed more sensitivity due to different vertical resolution than to the fine tuning of the drag constants. Therefore, after many calibration experiments, it is recommended to leave both drag constants unchanged. The vertical distribution of the zonal flow is well reproduced.

Together with the new sub-grid scale fields the bugfixes have a positive impact on the model climate. In particular geopotential height at 200hPa and 500hPa and MSLP improved over large areas. In contrast a slightly negative effect of the bugfixes was found when the old SGO fields were used. Zonal mean momentum flux and eddy heat flux are improved with the new fields.

The impact on forecast experiments in the medium range (with 31 levels) is neutral[1]. However, the 60 level 10-day forecast series showed a beneficial impact for the Northern Hemisphere in particular over the E-Asia and the North Pacific.

The spectral terrain analysis confirmed the importance of scale separation i.e. it is necessary to cut off the scales at some wavelength for the slope computation. Without scale separation the slope would be enhanced by a factor of 9 related to the old fields. The procedure of taking central differences for derivatives of terrain height from the fields at 2'30" resolution might not be optimal as a cutoff at the desired scale of about 5 km. Better spectral filtering techniques may be tried in future.

Blocking frequency has not been considered in this study, but it is known that mountain drag affects this parameter. In future work on orography, blocking frequency should be included.

Finally, the spectral terrain analysis with 3" data confirmed that slope parameters do not converge with very fine resolution. This is important for the boundary layer parametrization, where the slope of the small scale orographic features is relevant for the roughness length parametrization.

Acknowledgements

Discussions and reviews by Anton Beljaars and Martin Miller are gratefully acknowledged. Many helpful suggestions by Pedro Viterbo and Agathe Untch are also acknowledged. Special thanks to Bodo Ritter for finding bugs and Cedo Brankovic for generating plots for zonal mean eddy fluxes.

[1]Since the work discussed in this memo, the impact of the new subgrid orography fields has been extensively tested as part of model cycle 21R4 introduced on 12-10-1999. In general the impact was positive and contributed to the large overall improvement obtained in this cycle (see ECMWF Newsletter nr. 87, Spring 2000)

References

Bannon, P. R. and Yuhas, J. A. 1990: On montain wave drag over complex terrain. *Meteorol. Atmos. Phys.*, **43**, 155-162

Gesch, D. B. and Larson, K. S., 1998: Techniques for development of global 1-kilometer digital elevation models, in *Proceedings, Pecora Thirteen Symposium*, Sioux Falls, South Dakota, August 20-22, 1996 (CD-ROM), Am. Soc. for Photogrammetry and Remote Sens., Bethesda, Md.

Gilbert, L. E., 1989: Are topographic data sets fractal? *PAGEOPH.*, **131**,241-254.

Ekholm, S., 1996: A full coverage, high-resolution topographic model of Greenland computed from a variety of digital elevatation data. *Journal of Geophysical Research* **101** (B10), 21961-21972.

Lott, F., and Miller M., 1997: A new sub-grid scale orographic drag parametrization; its testing in the ECMWF model *Quart. J. Roy. Meteor. Soc.*, 123, 101-127.

Mengesha, Y. G., 1997: Studies on parametrization of sub-grid scale topography for atmospheric models. Submitted to Cress Research Evalutation Course (REC).

Miller, M. J., Palmer, T. N. and Swinbank, R. 1989: Parametrization and influence of sub-grid scale orography in general circulation and numerical weather prediction models. *Meteorol. Atmos. Phys.*, **40**, 84-109

Palmer, T. N., Shutts, G. J. and Swinbank, R., 1986: Alleviation of systematic westerly bias in general circulation and numerical weather prediction models through an orographic gravity wave drag parametrization. *Quart. J. Roy. Meteor. Soc.*, **112**, 1001-1039

Phillips, S. P., 1984: Analytical surface pressure and drag for linear hydrostatic flow over three-dimensional elliptical mountains. *J. Atmos. Sci.*, **41**, 1073-1084.

Smith, R. B. and Gleason, A., 1997: private communication.

Steinwand, D. R., Hutchinson, J. A., and Snyder, J. P., 1995: Map projections for global and continental data sets and an analysis of pixel distortion caused by reprojection, Photogrammetric Engineering and Remote Sensing, **61**, 1915-1924.

Steyn and Ayotte, 1985: Application of a two-dimensional terrain height Spectra to Mesoscale Modeling, *J. Atmos. Sci.* **42**(24), 2884-2887.

Taylor, P. A., 1997: Boundary-Layer modelling of neutral and stably-stratified flow over hills, with emphasis on the drag. Procedings of a Workshop held at ECMWF on Orography, Reading, November 10-12, 1997, ECMWF WORKSHOP PROCEEDINGS.

Working Group Report: Procedings of a Workshop held at ECMWF on Orography, Reading, November 10-12, 1997, ECMWF WORKSHOP PROCEEDINGS.

Young, G. S., and Pielke, R. A.,1983: Application of terrain height variance spectra to mesoscale modeling, *J. Atmos. Sci.* **40**(10), 2555-2560.

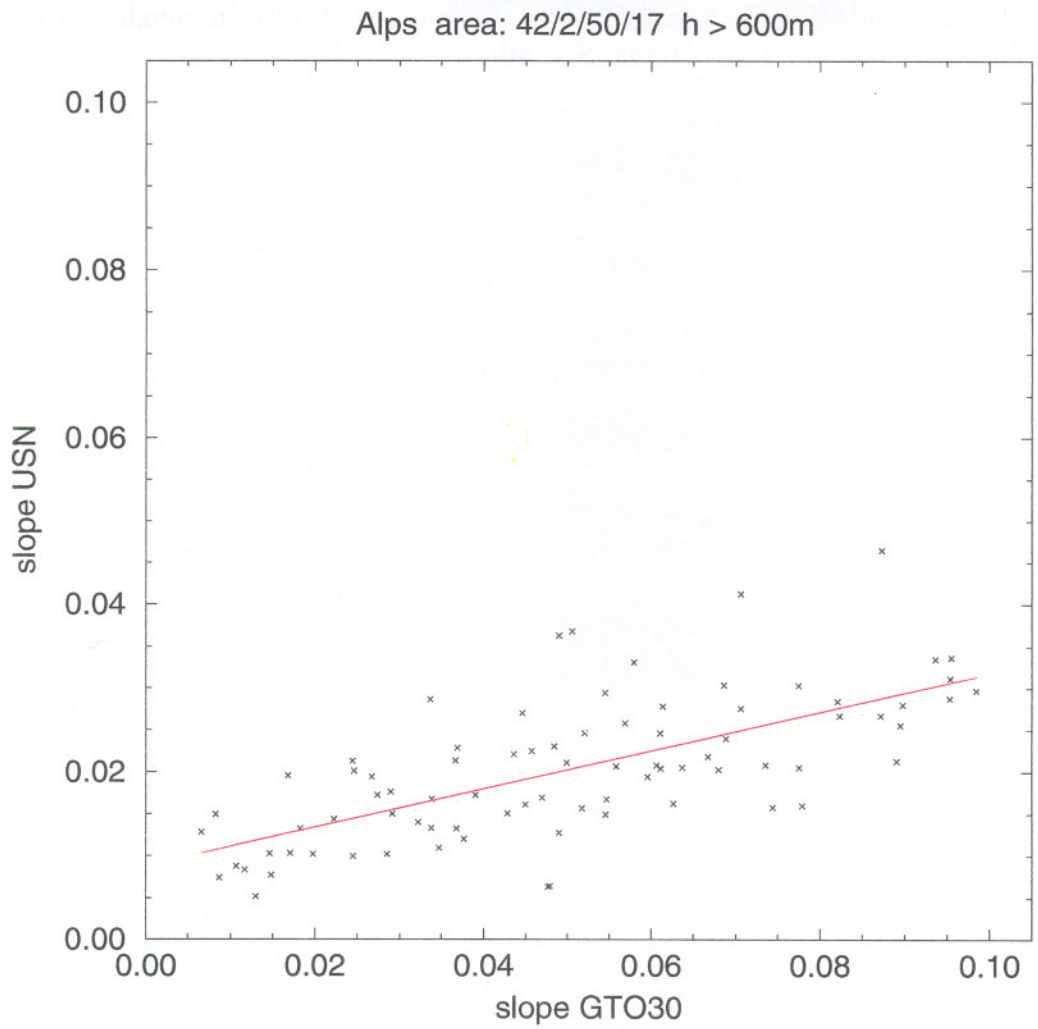

Figure 1: Scatter plots of slope from 10 arcmin data (US-Navy) against 30 arcsec data (GTOPO30) for the area between 42°to 50°N and 2°to 17°E

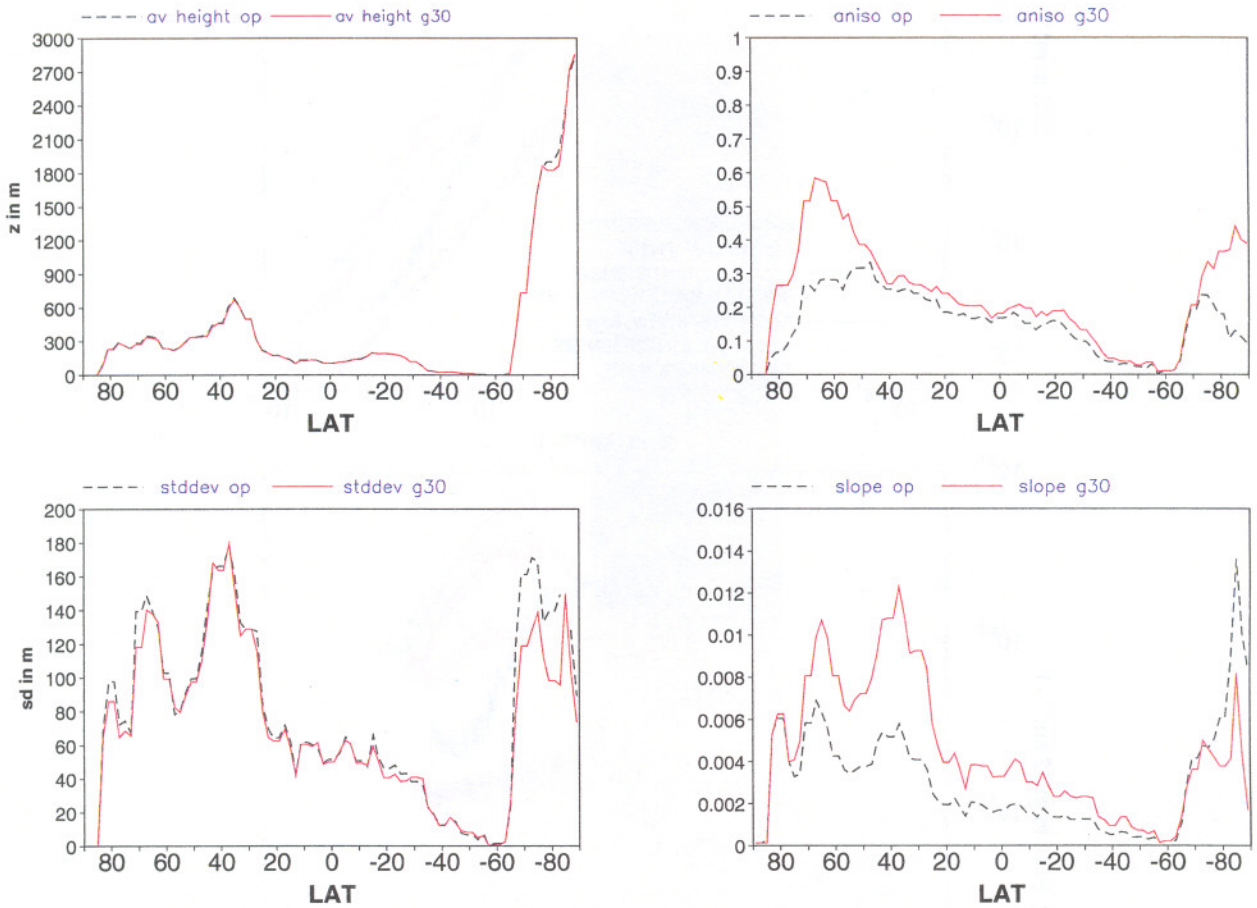

Figure 2: Zonal means for height (top left), standard deviation (bottom left), anisotropy (isotropic=1; top right) and slope (bottom right) averaged over a two degree latitude band. The GTOPO30 derived fields are represented by the solid lines; the US-Navy derived fields by the dashed lines.

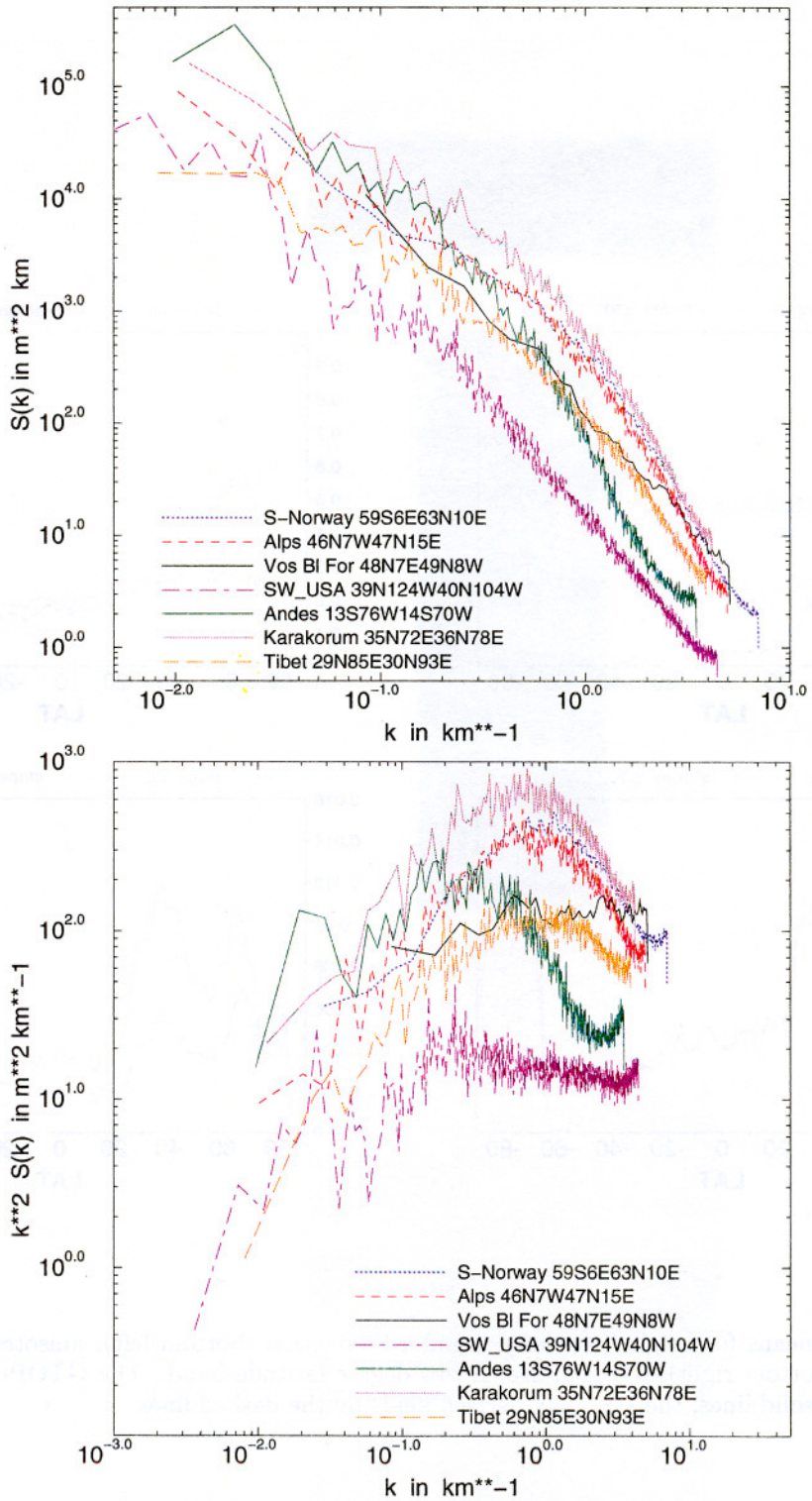

Figure 3: W-E variance spectra (top panel) and slope spectra (bottom panel) from the 30" GTOPO30 terrain height data for various regions

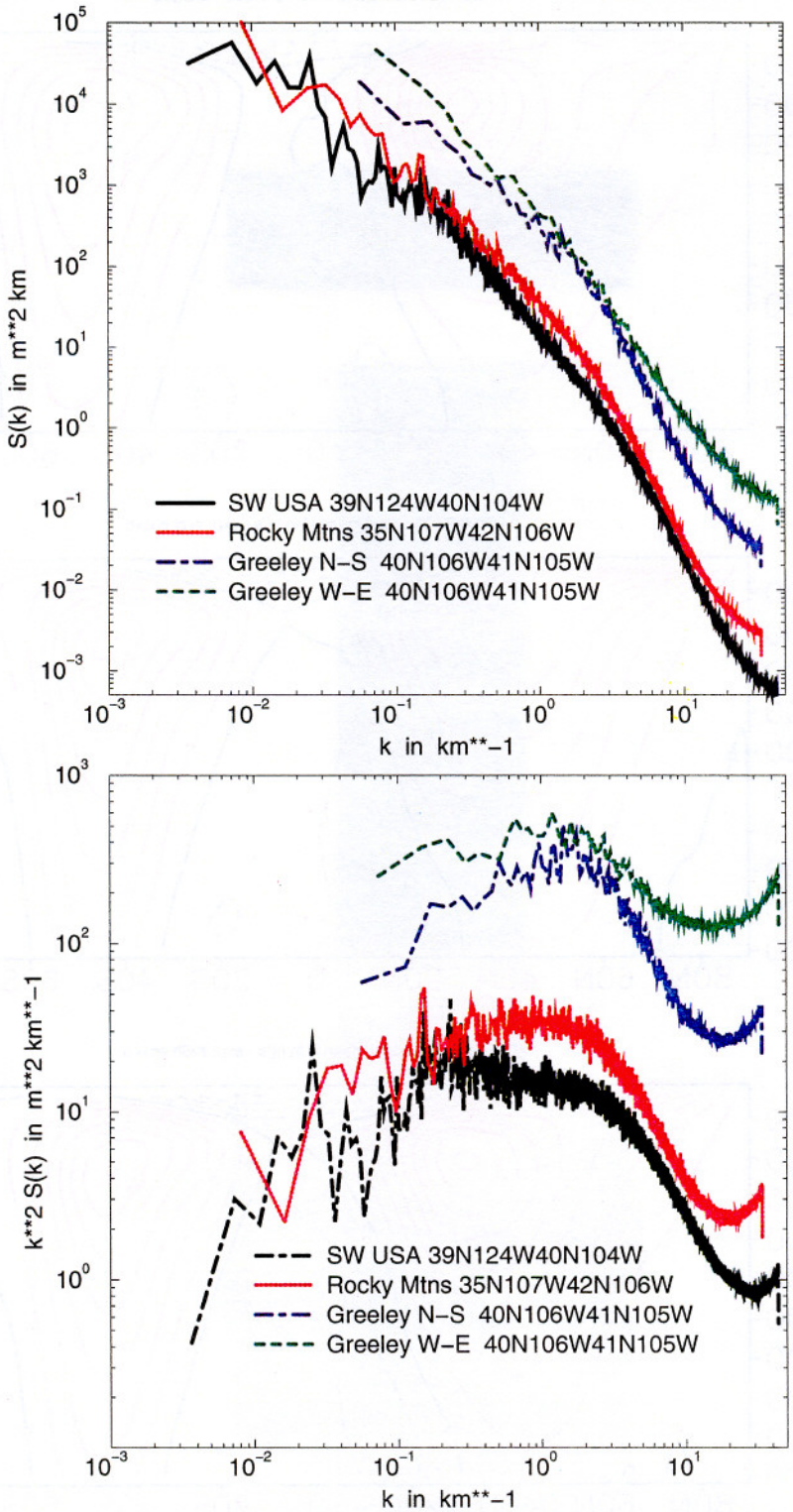

Figure 4: Variance spectra (top panel) and slope spectra (bottom panel) from 3" terrain height data for different cross-sections: West coast - Continental Divide, N-S along the Rocky Mountains near Denver and Greeley (Rocky Mountains near Denver).

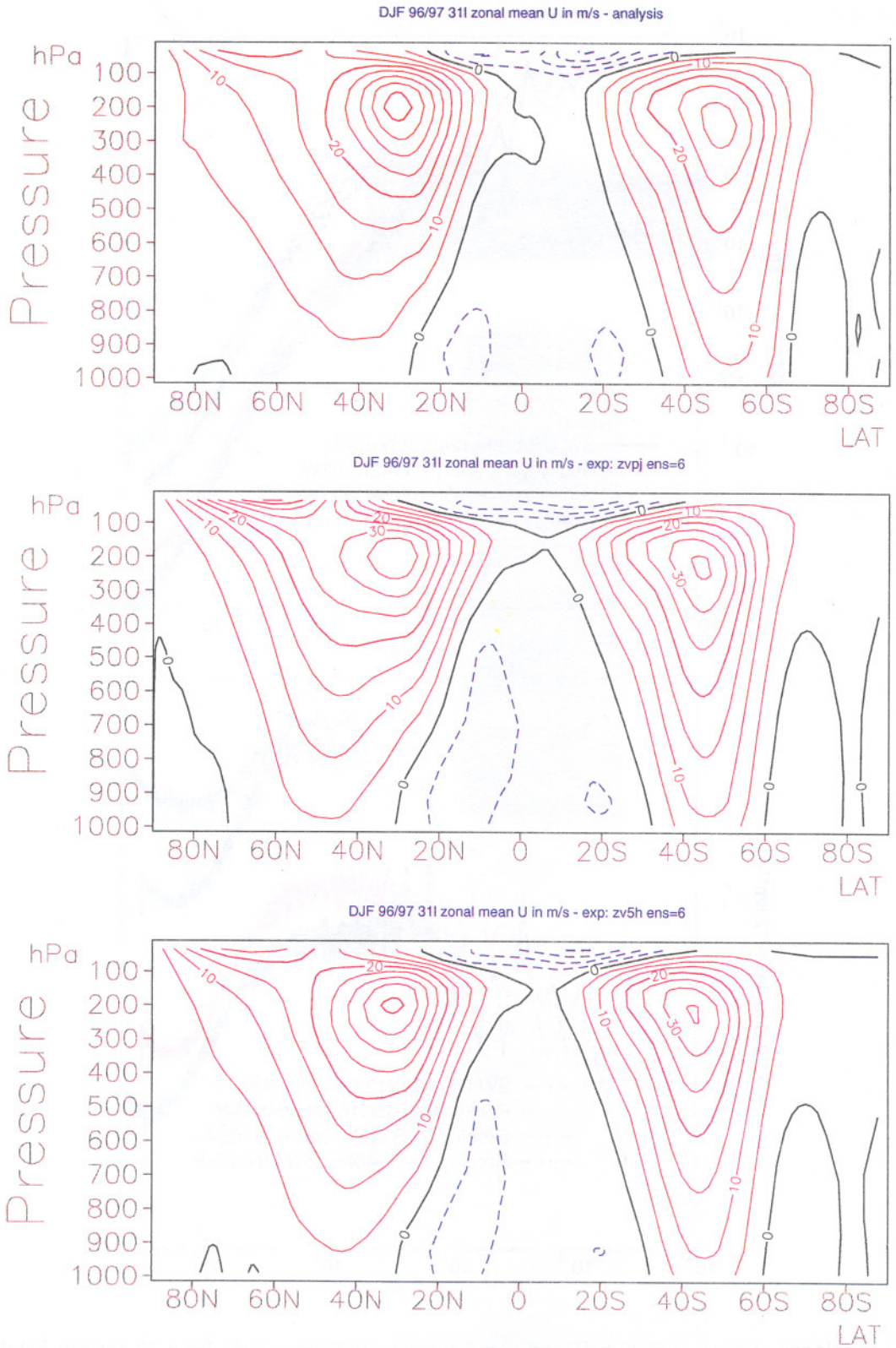

Figure 5: Zonal mean wind for DJF 96/97 from the analysis (top panel), the experiment without SGO scheme (middle panel, zvpj), and the control experiment with SGO scheme using the old US-Navy fields (lower panel, zv5h).

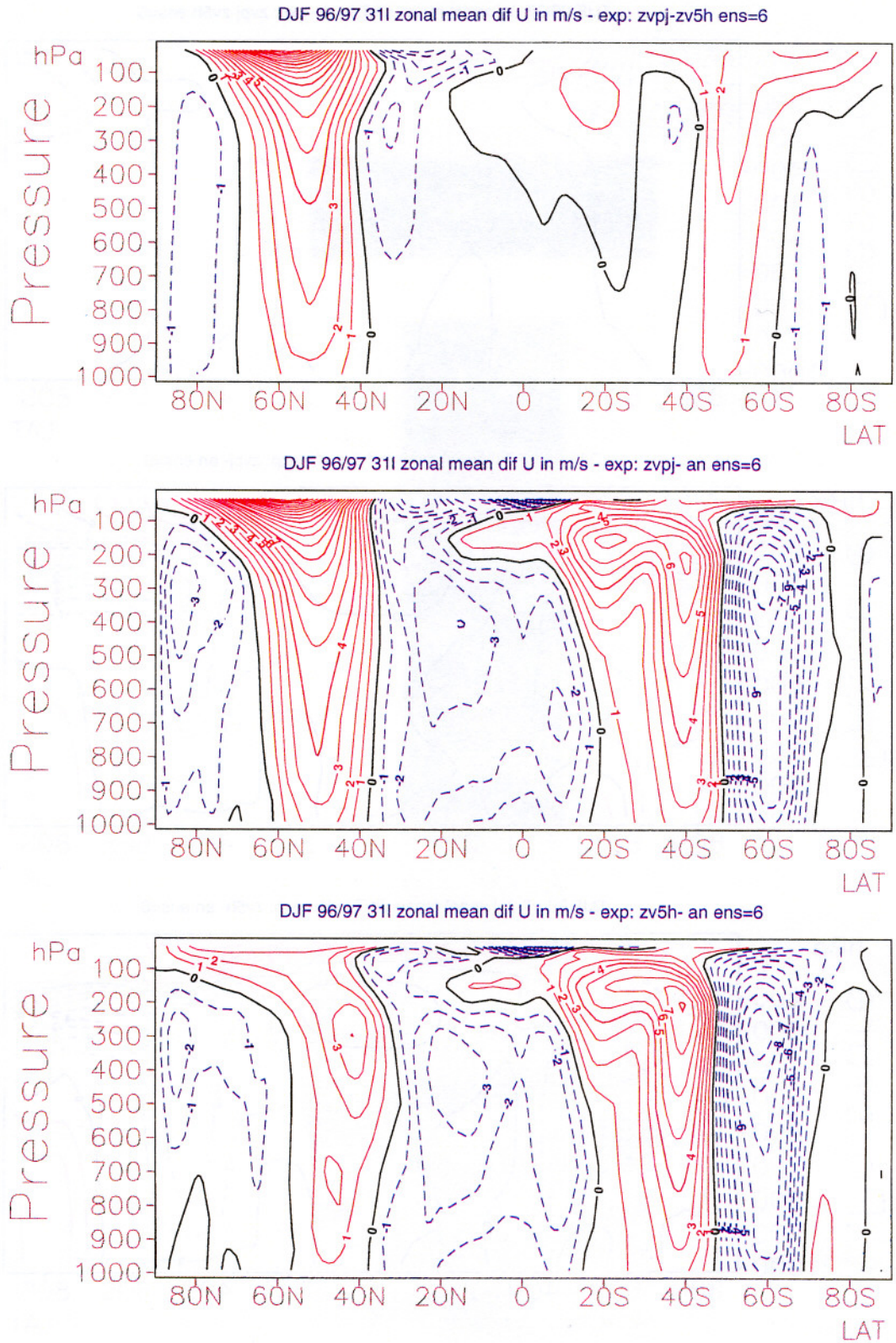

Figure 6: Zonal mean wind differences and errors for DJF 96/97. The top panel represent the difference between the experiments without SGO scheme and the control (zvpj-zv5h), the middle panel the error of the experiment without SGO scheme (zvpj-ana), and the bottom panel the error of the control experiment (zv5h-ana).

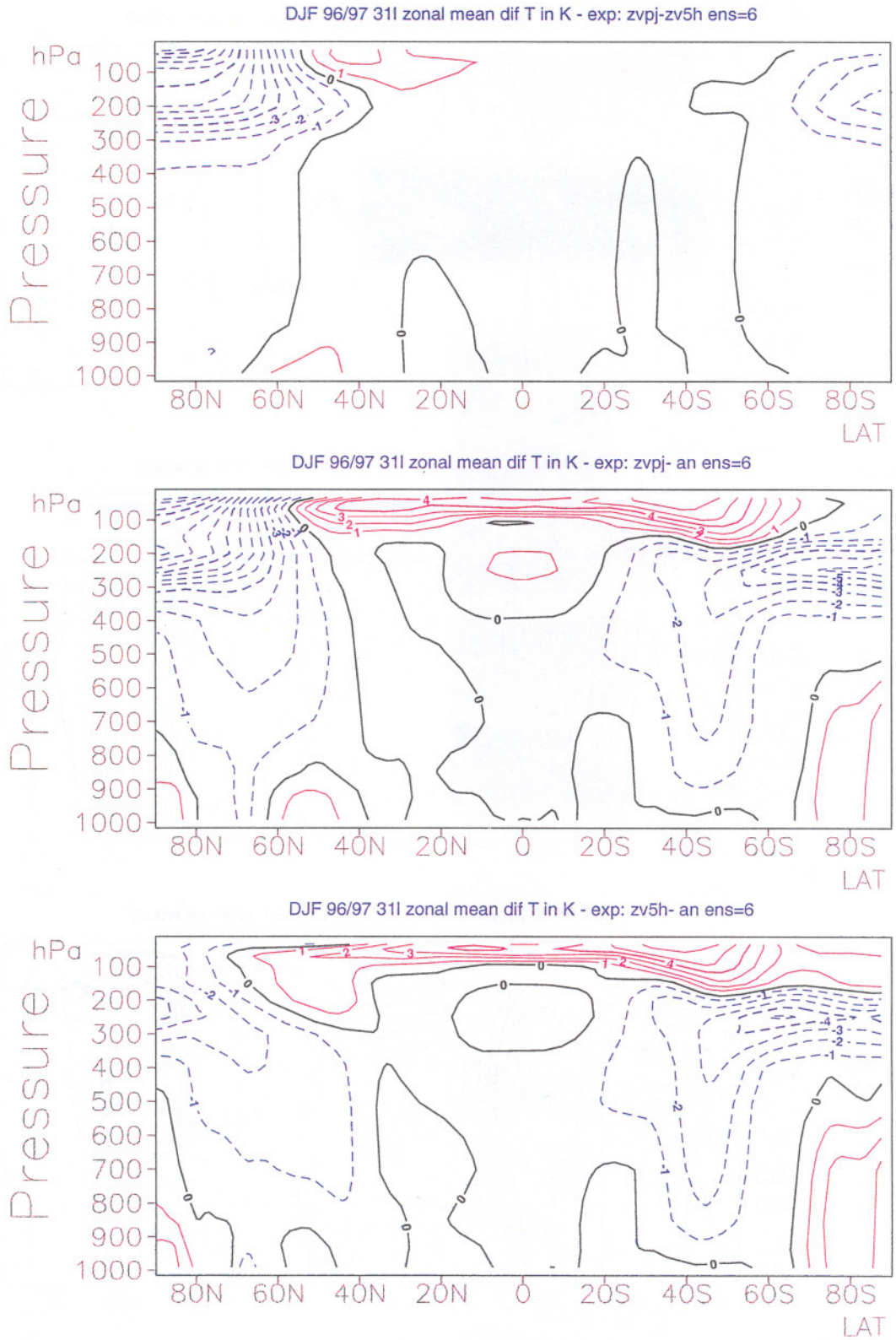

Figure 7: Zonal mean temperature differences and errors for DJF 96/97. The top panel represent the difference between the experiments without SGO scheme and the control (zvpj-zv5h), the middle panel the error of the experiment without SGO scheme (zvpj-ana), and the bottom panel the error of the control experiment (zv5h-ana).

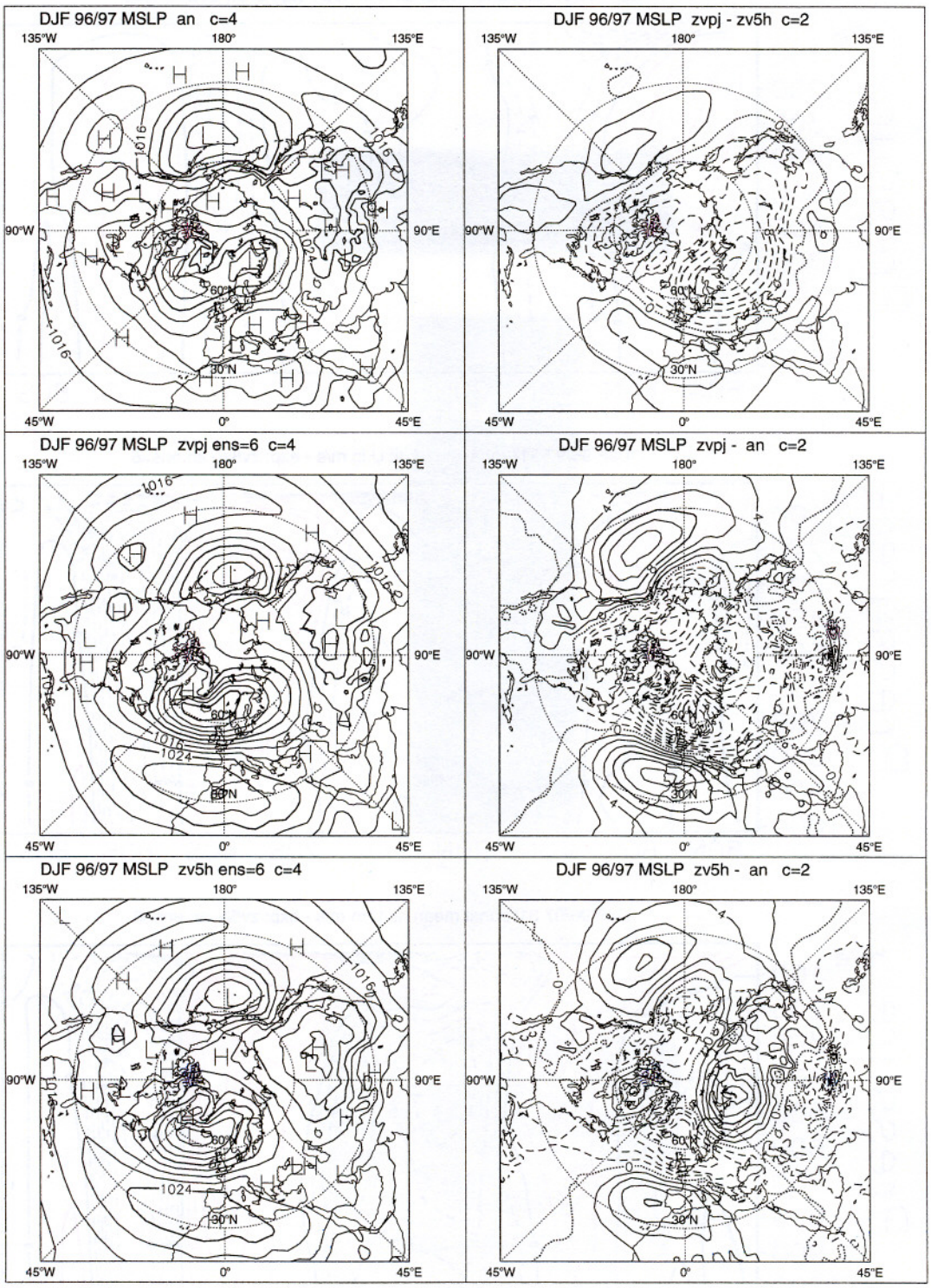

Figure 8: Mean sea level pressure verification for DJF 96/97 (contour interval: 4 hPa for full fields and 2 hPa for differences and errors). The panels represent: analysis (ana, top left), experiment without SGO scheme (zvpj, middle left), control experiment (zv5h, bottom left), difference between experiments (zvpj-zv5h, top right), error of experiment without SGO scheme (zvpj-ana, middle right), and error of the control experiment (zv5h-ana, bottom right).

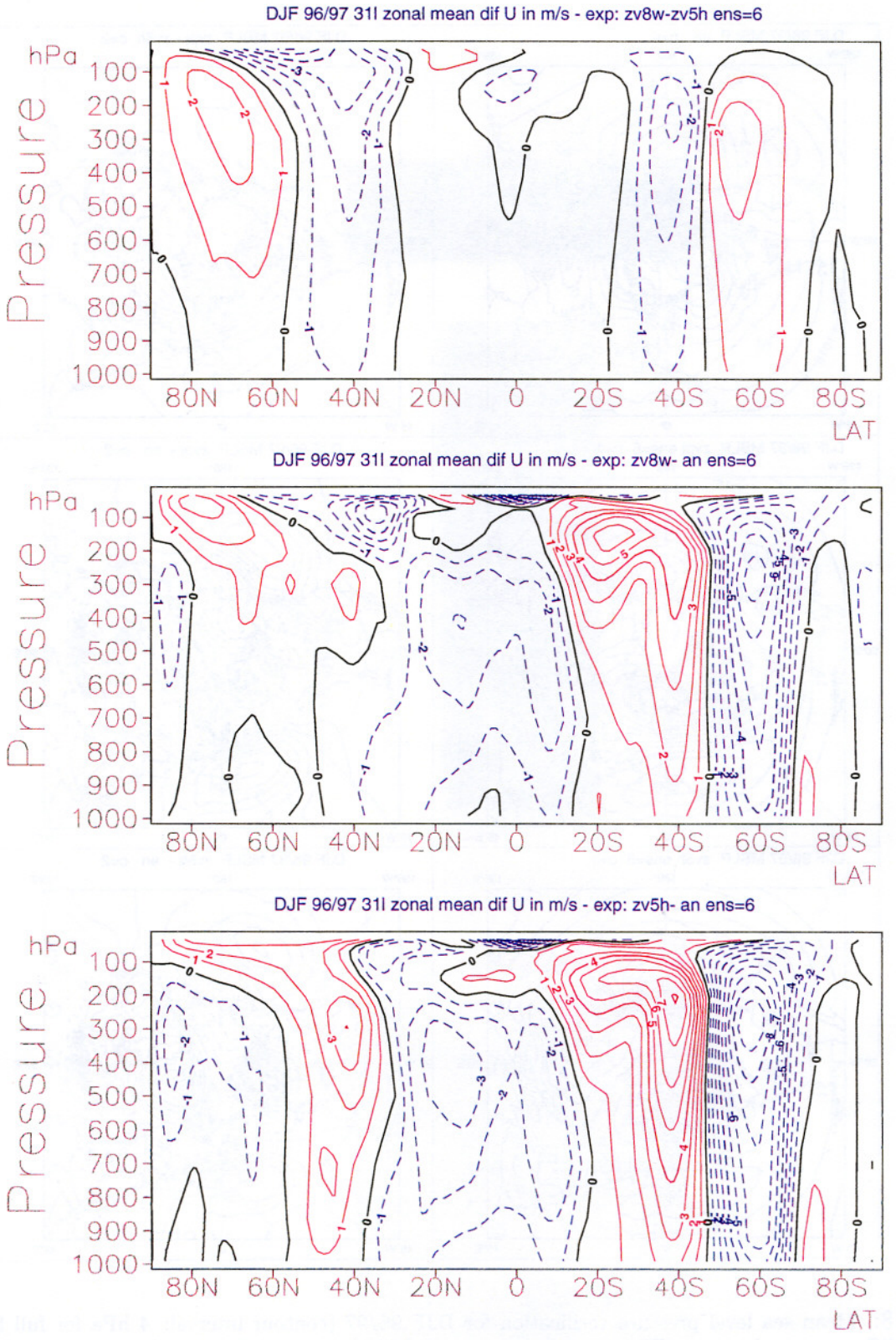

Figure 9: Zonal mean wind difference and errors for DJF 96/97. The top panel represent the difference between the experiments with the new SGO fields and the control (zv8w-zv5h), the middle panel the error of the experiment with new SGO fields (zv8w-ana), and the bottom panel the error of the control experiment (zv5h-ana).

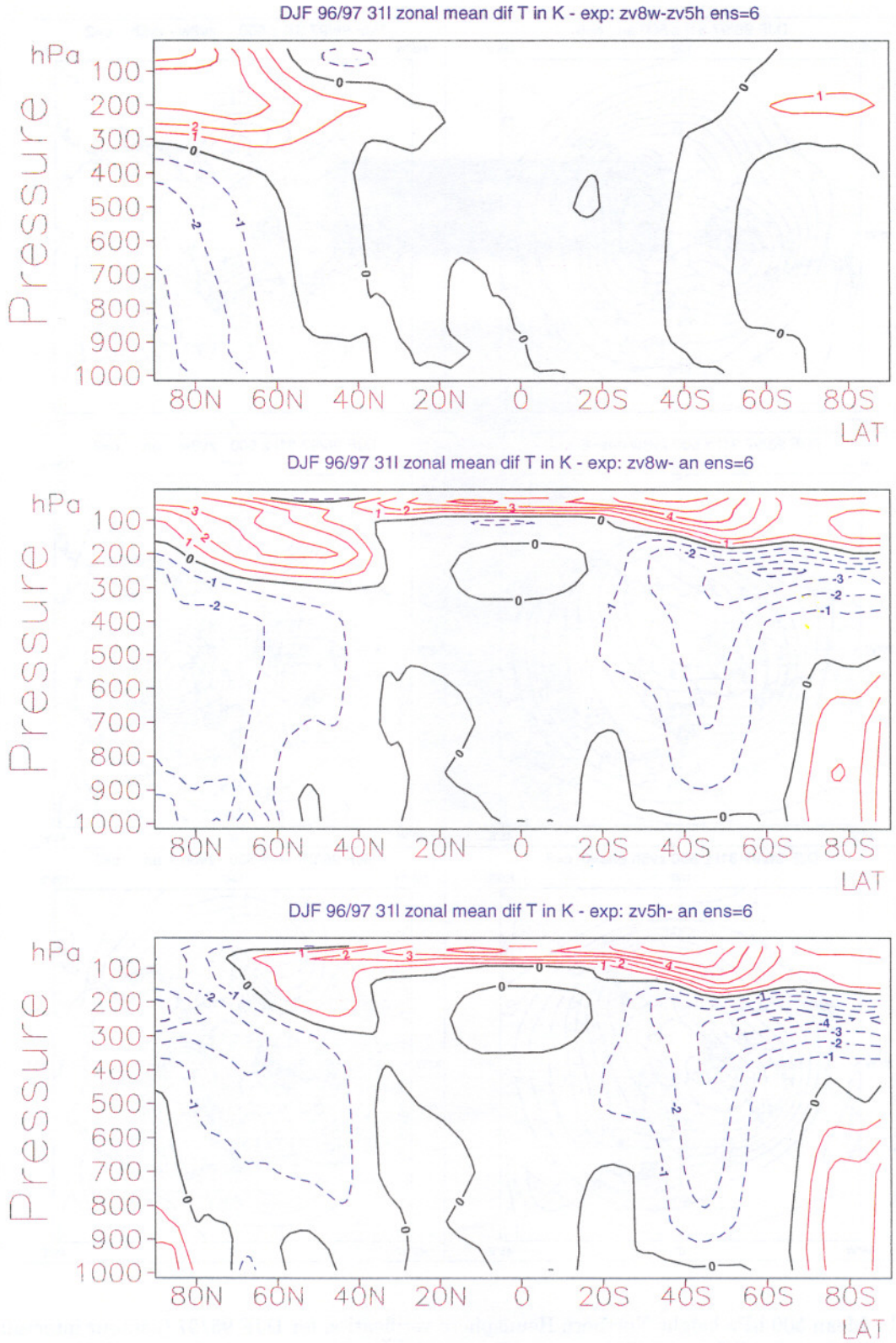

Figure 10: Zonal mean temperature difference and errors for DJF 96/97. The top panel represent the difference between the experiments with the new SGO fields and the control (zv8w-zv5h), the middle panel the error of the experiment with new SGO fields (zv8w-ana), and the bottom panel the error of the control experiment (zv5h-ana).

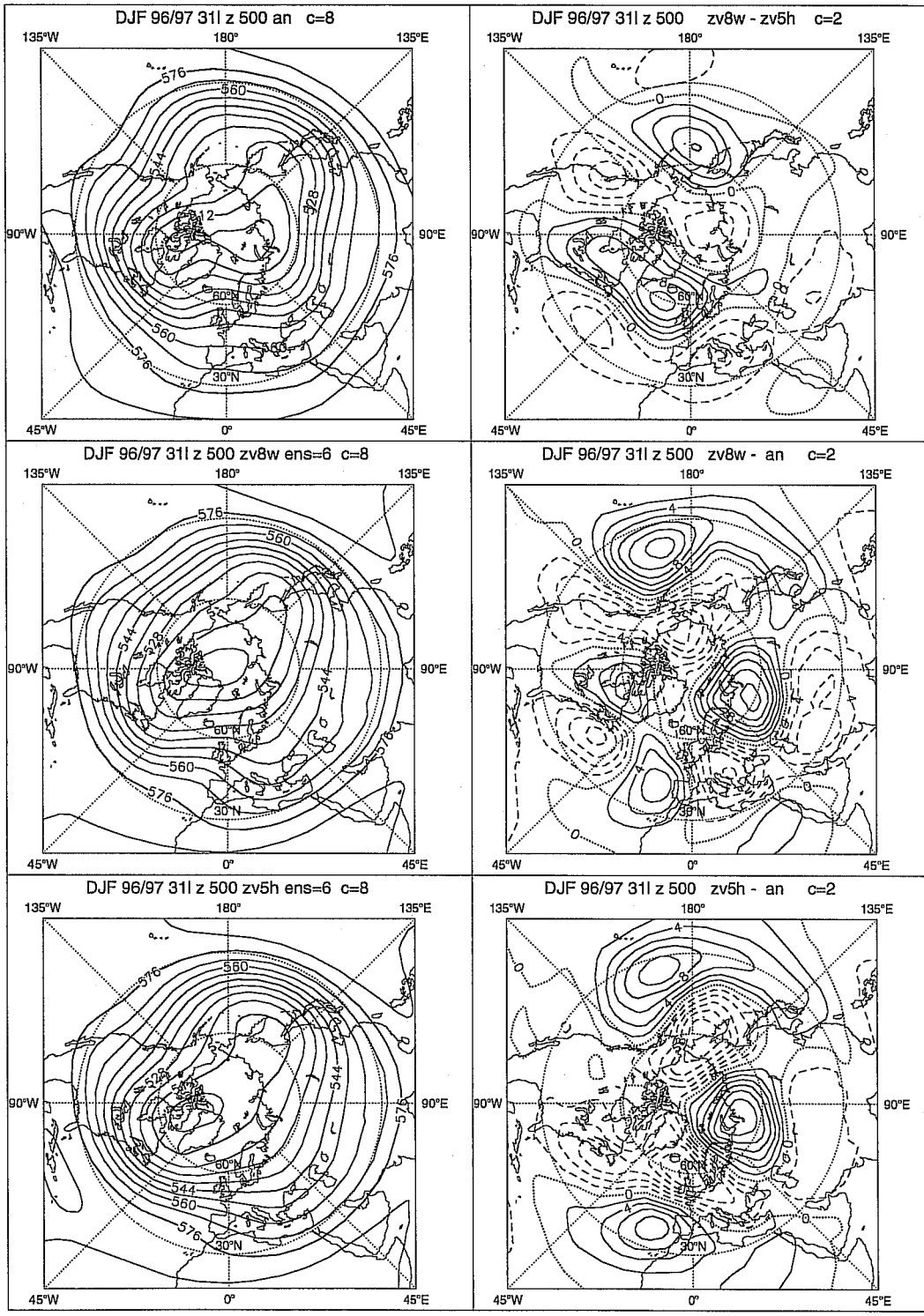

Figure 11: Mean 500 hPa height Northern Hemisphere verification for DJF 96/97 (contour interval: 8 dam for full fields and 2 dam for differences and errors). The panels represent: analysis (ana, top left), experiment with new SGO fields (zv8w, middle left), control experiment (zv5h, bottom left), difference between experiments (zv8w-zv5h, top right), error of experiment with new SGO fields (zv8w-ana, middle right), and error of the control experiment (zv5h-ana, bottom right).

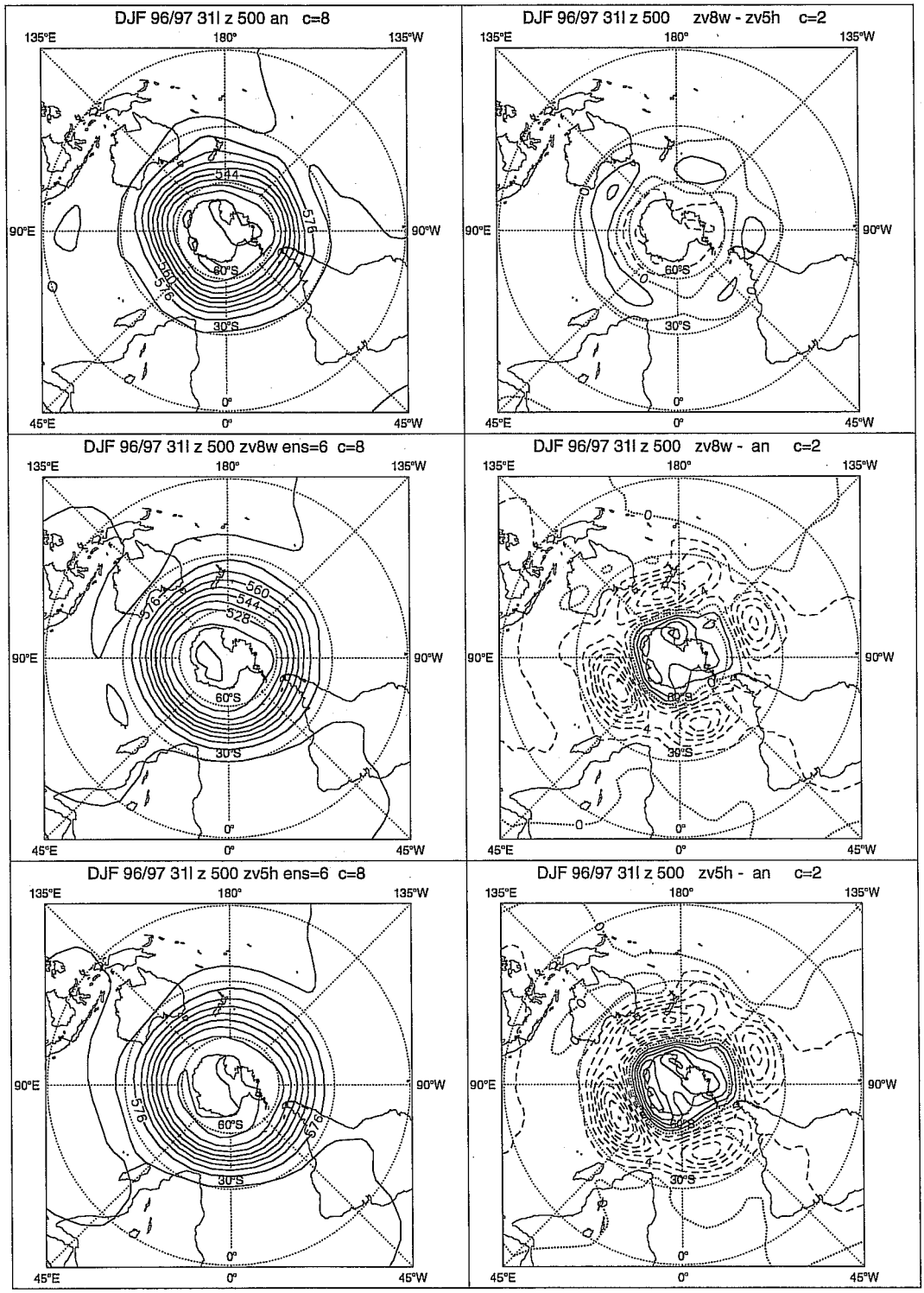

Figure 12: Mean 500 hPa height Southern Hemisphere verification for DJF 96/97 (contour interval: 8 dam for full fields and 2 dam for differences and errors). The panels represent: analysis (ana, top left), experiment with new SGO fields (zv8w, middle left), control experiment (zv5h, bottom left), difference between experiments (zv8w-zv5h, top right), error of experiment with new SGO fields (zv8w-ana, middle right), and error of the control experiment (zv5h-ana, bottom right).

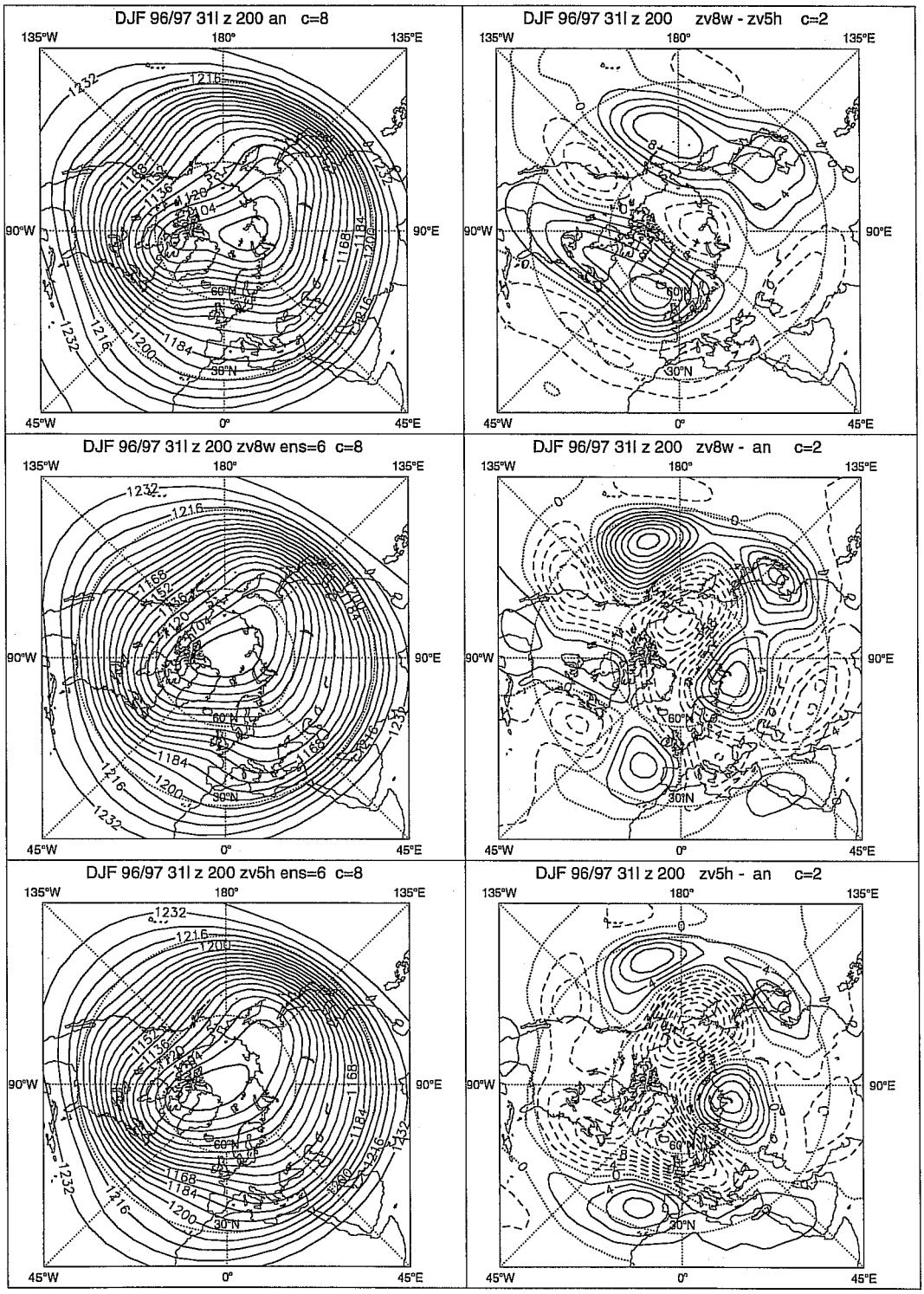

Figure 13: Mean 200 hPa height Northern Hemisphere verification for DJF 96/97 (contour interval: 8 dam for full fields and 2 dam for differences and errors). The panels represent: analysis (ana, top left), experiment with new SGO fields (zv8w, middle left), control experiment (zv5h, bottom left), difference between experiments (zv8w-zv5h, top right), error of experiment with new SGO fields (zv8w-ana, middle right), and error of the control experiment (zv5h-ana, bottom right).

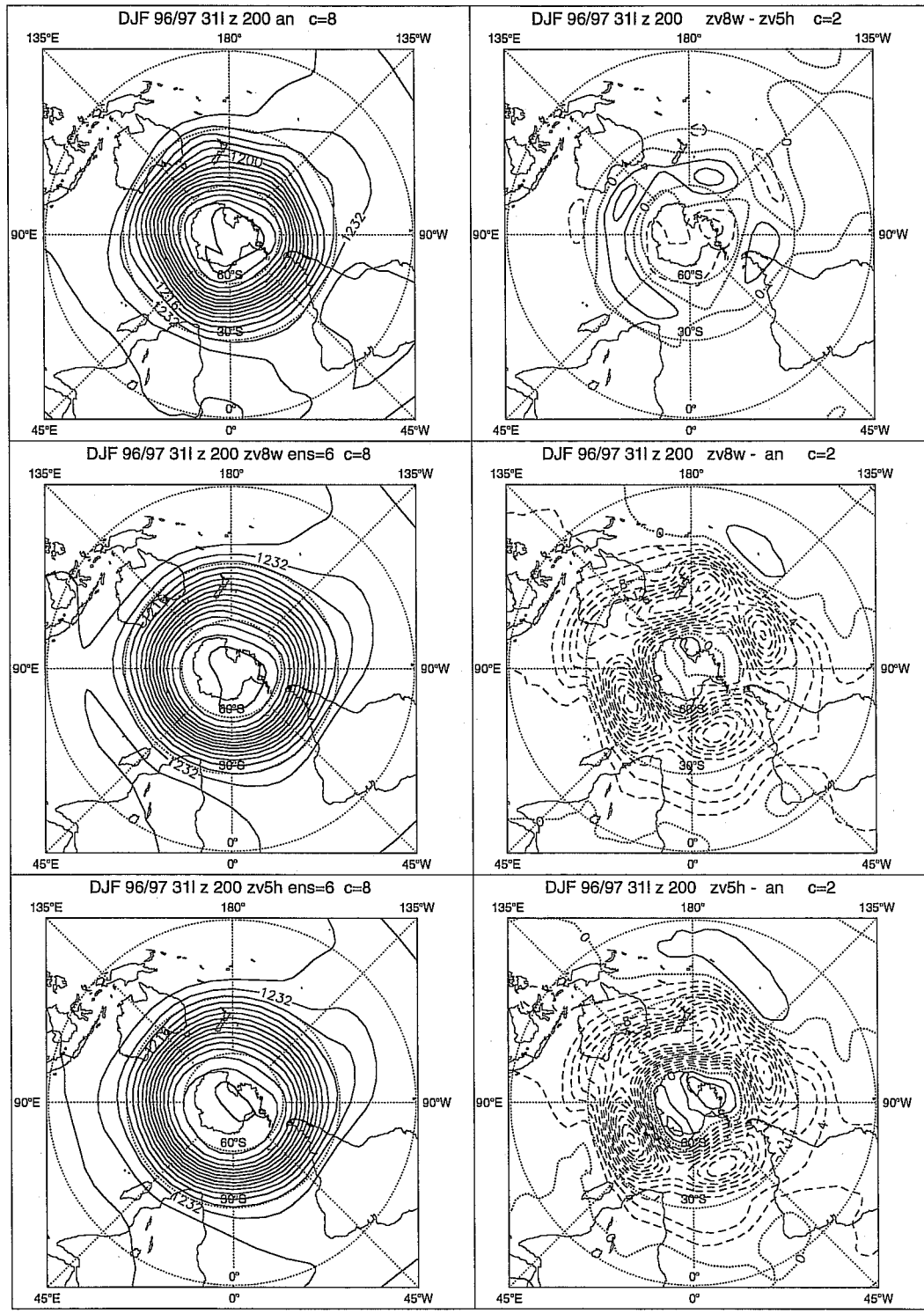

Figure 14: Mean 200 hPa height Southern Hemisphere verification for DJF 96/97 (contour interval: 8 dam for full fields and 2 dam for differences and errors). The panels represent: analysis (ana, top left), experiment with new SGO fields (zv8w, middle left), control experiment (zv5h, bottom left), difference between experiments (zv8w-zv5h, top right), error of experiment with new SGO fields (zv8w-ana, middle right), and error of the control experiment (zv5h-ana, bottom right).

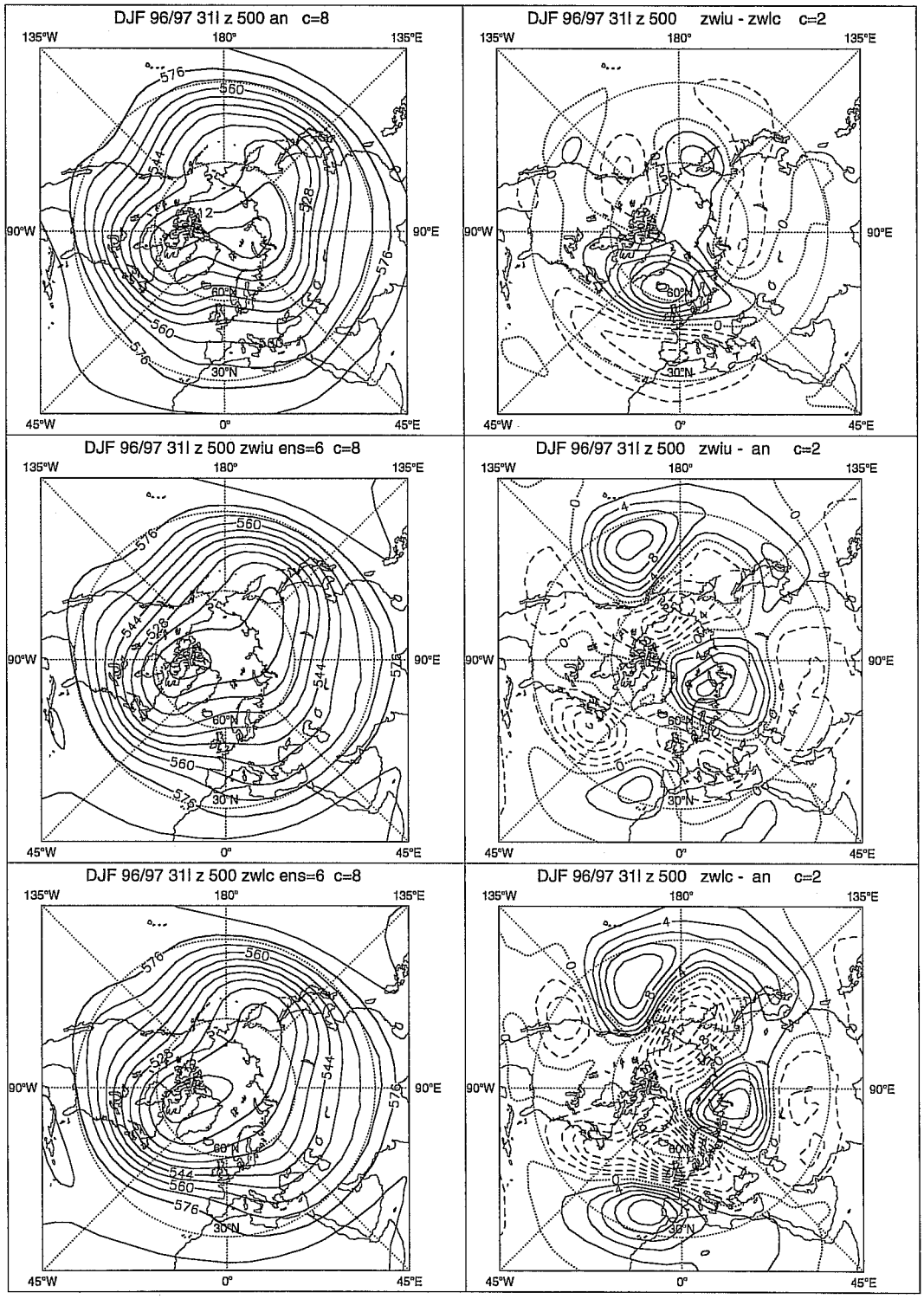

Figure 15: Mean 500 hPa height Northern Hemisphere verification for DJF 96/97 (contour interval: 8 dam for full fields and 2 dam for differences and errors). The panels represent: analysis (ana, top left), experiment with new SGO fields (zwiu, middle left), control experiment (zwlc, bottom left), difference between experiments (zwiu-zwlc, top right), error of experiment with new SGO fields (zwiu-ana, middle right), and error of the control experiment (zwlc-ana, bottom right). Both experiments use the corrected code.

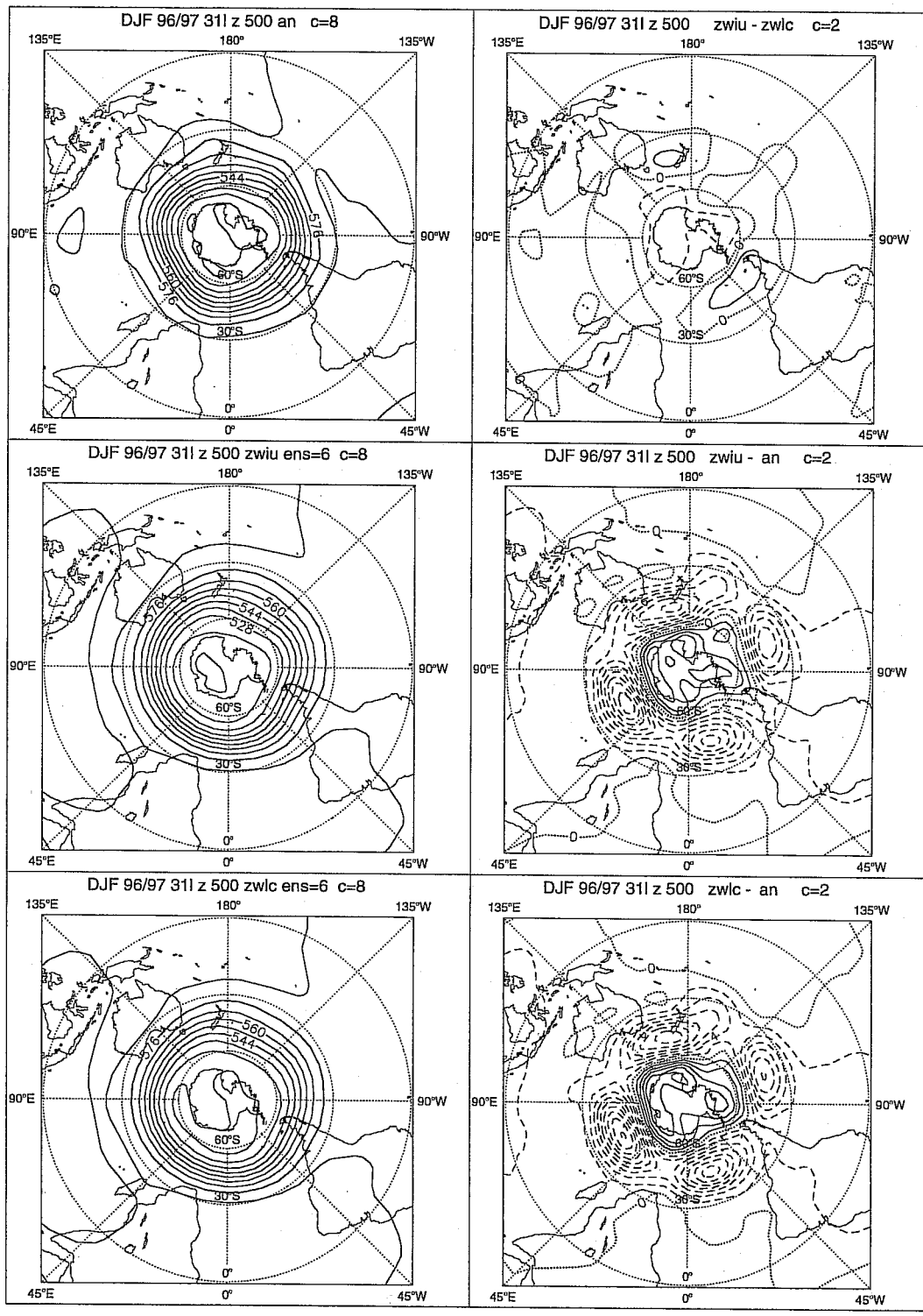

Figure 16: Mean 500 hPa height Southern Hemisphere verification for DJF 96/97 (contour interval: 8 dam for full fields and 2 dam for differences and errors). The panels represent: analysis (ana, top left), experiment with new SGO fields (zwiu, middle left), control experiment (zwlc, bottom left), difference between experiments (zwiu-zwlc, top right), error of experiment with new SGO fields (zwiu-ana, middle right), and error of the control experiment (zwlc-ana, bottom right). Both experiments use the corrected code.

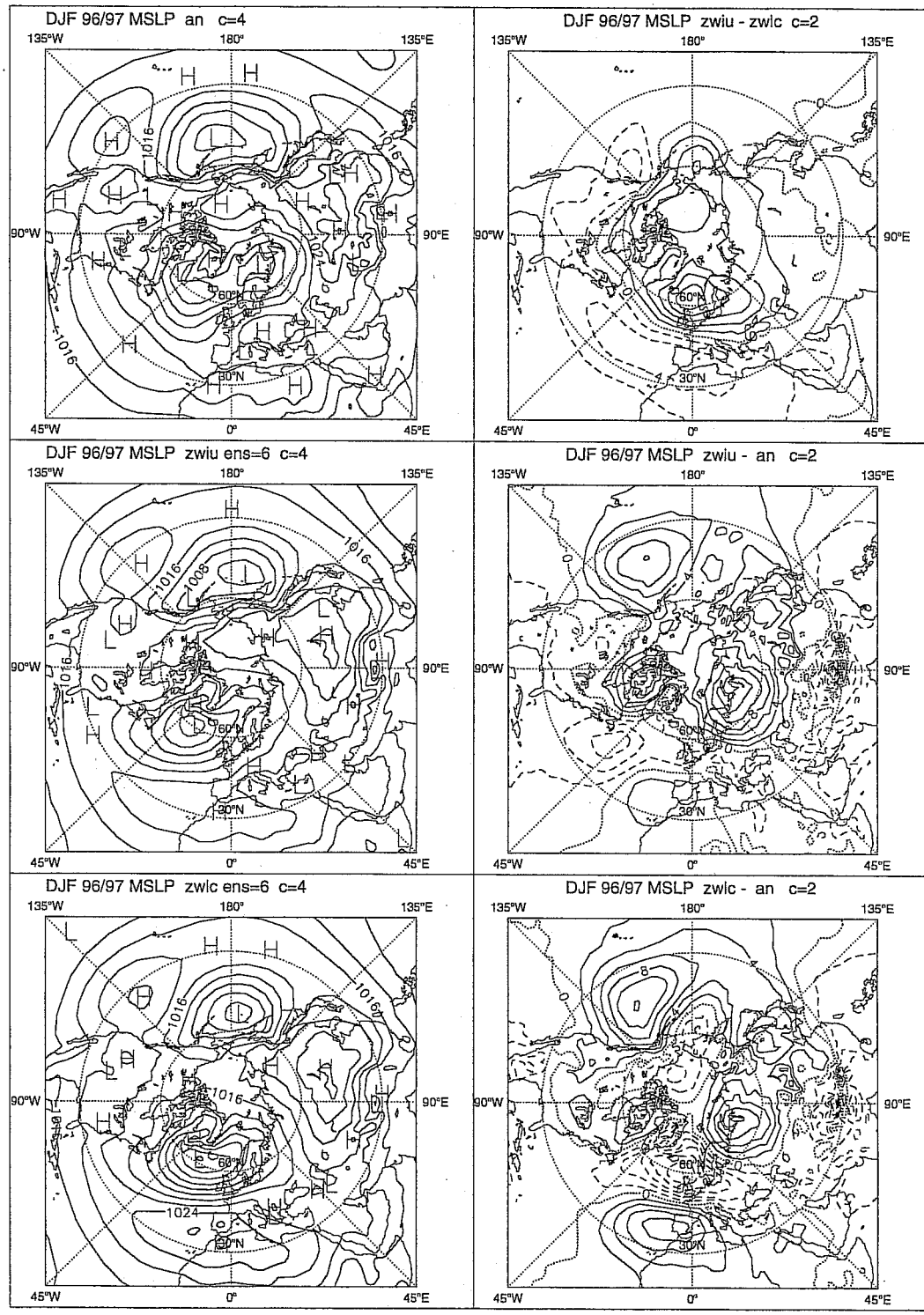

Figure 17: Mean sea level pressure Northern Hemisphere verification for DJF 96/97 (contour interval: 4 hPa for full fields and 2 hPa for differences and errors). The panels represent: analysis (ana, top left), experiment with new SGO fields (zwiu, middle left), control experiment (zwlc, bottom left), difference between experiments (zwiu-zwlc, top right), error of experiment with new SGO fields (zwiu-ana, middle right), and error of the control experiment (zwlc-ana, bottom right). Both experiments use the corrected code.

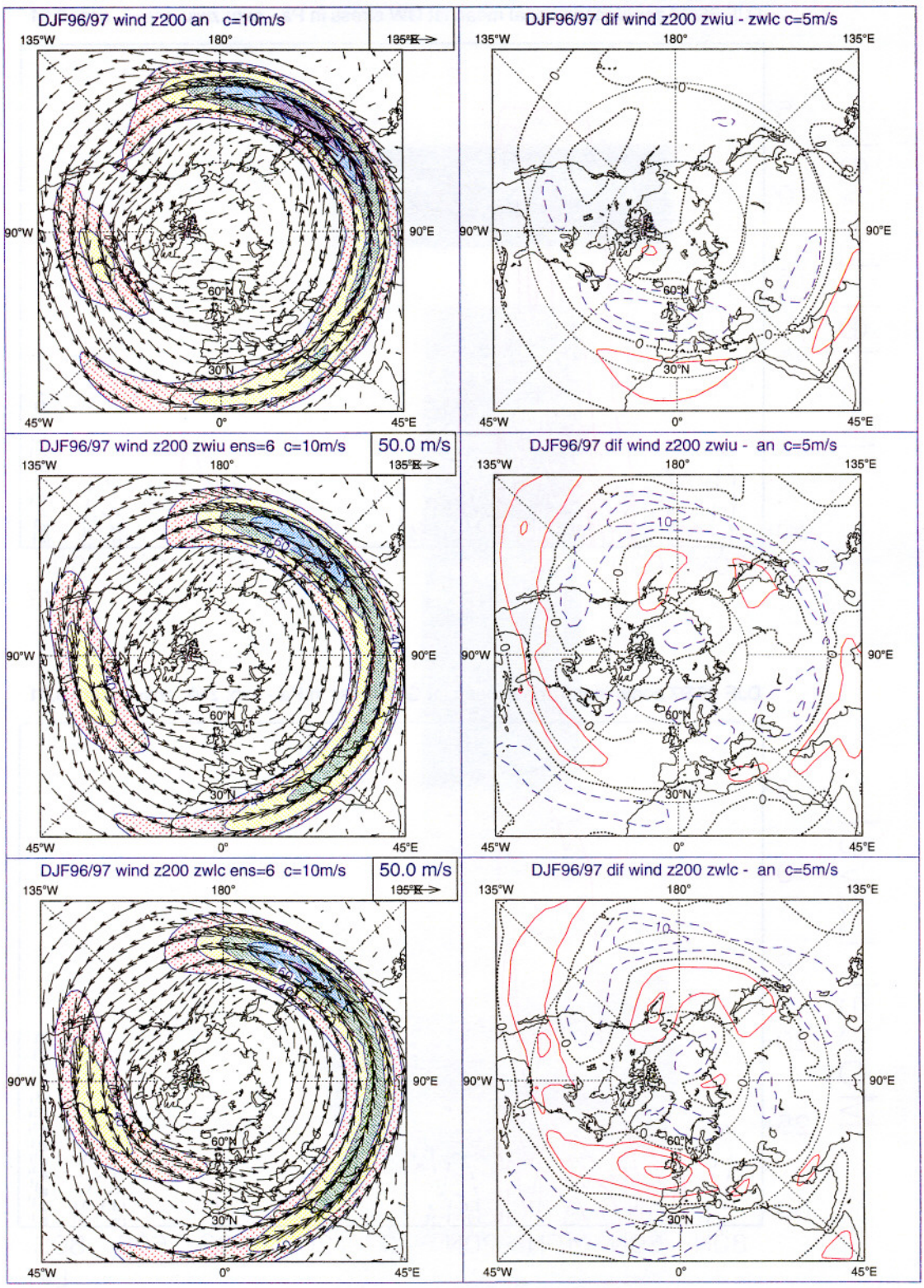

Figure 18: Northern Hemisphere 200 hPa wind verification for DJF 96/97 (contour interval: 10 m/s for full fields and 5 m/s for differences and errors). The panels represent: analysis (ana, top left), experiment with new SGO fields (zwiu, middle left), control experiment (zwlc, bottom left), difference between experiments (zwiu-zwlc, top right), error of experiment with new SGO fields (zwiu-ana, middle right), and error of the control experiment (zwlc-ana, bottom right). Both experiments use the corrected code.

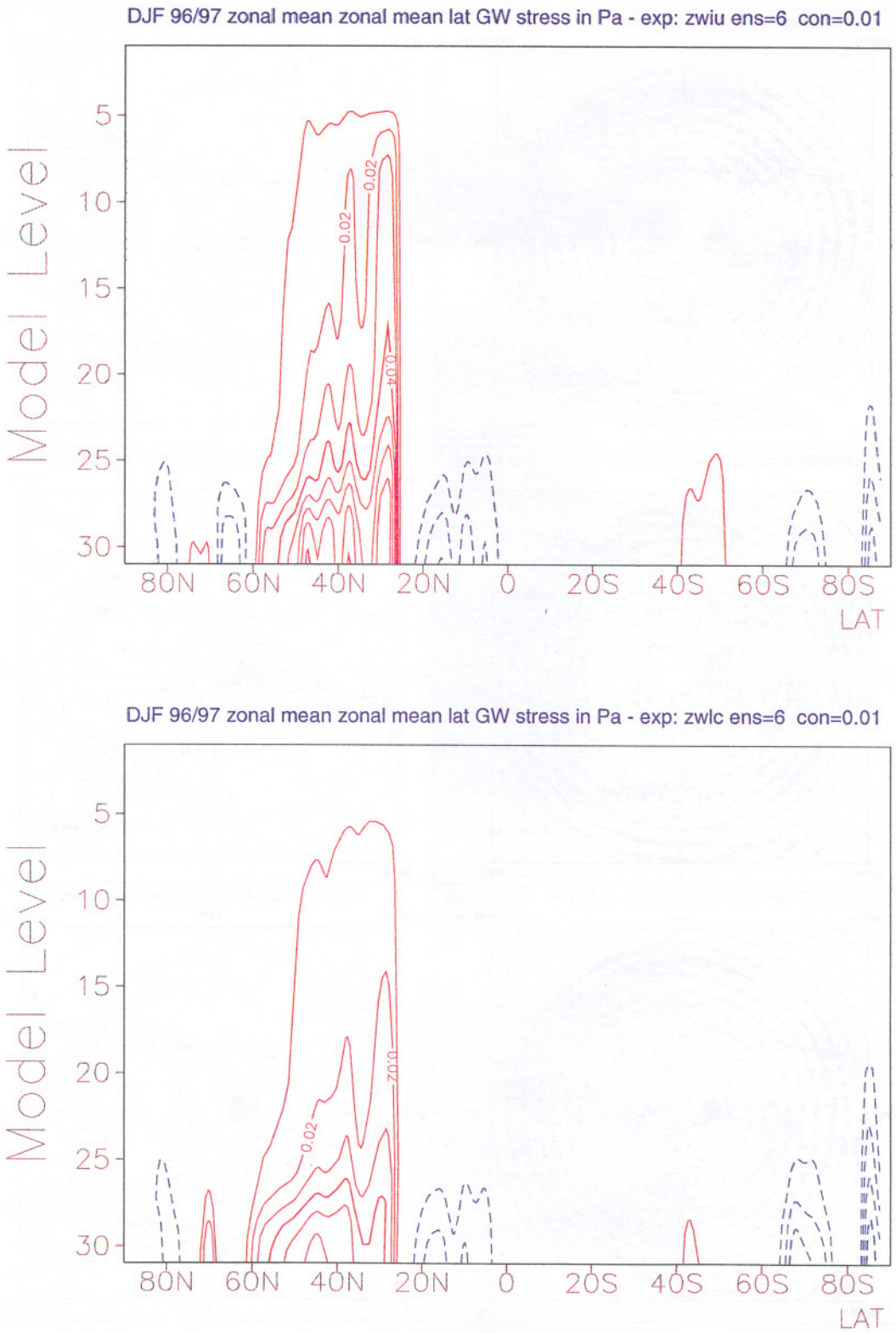

Figure 19: Zonal mean zonal gravity wave stress for (bugcorrected) experiments with new SGO fields (zwiu, top panel), and old fields (zwlc, bottom panel). Contour interval: 0.01 Pa.

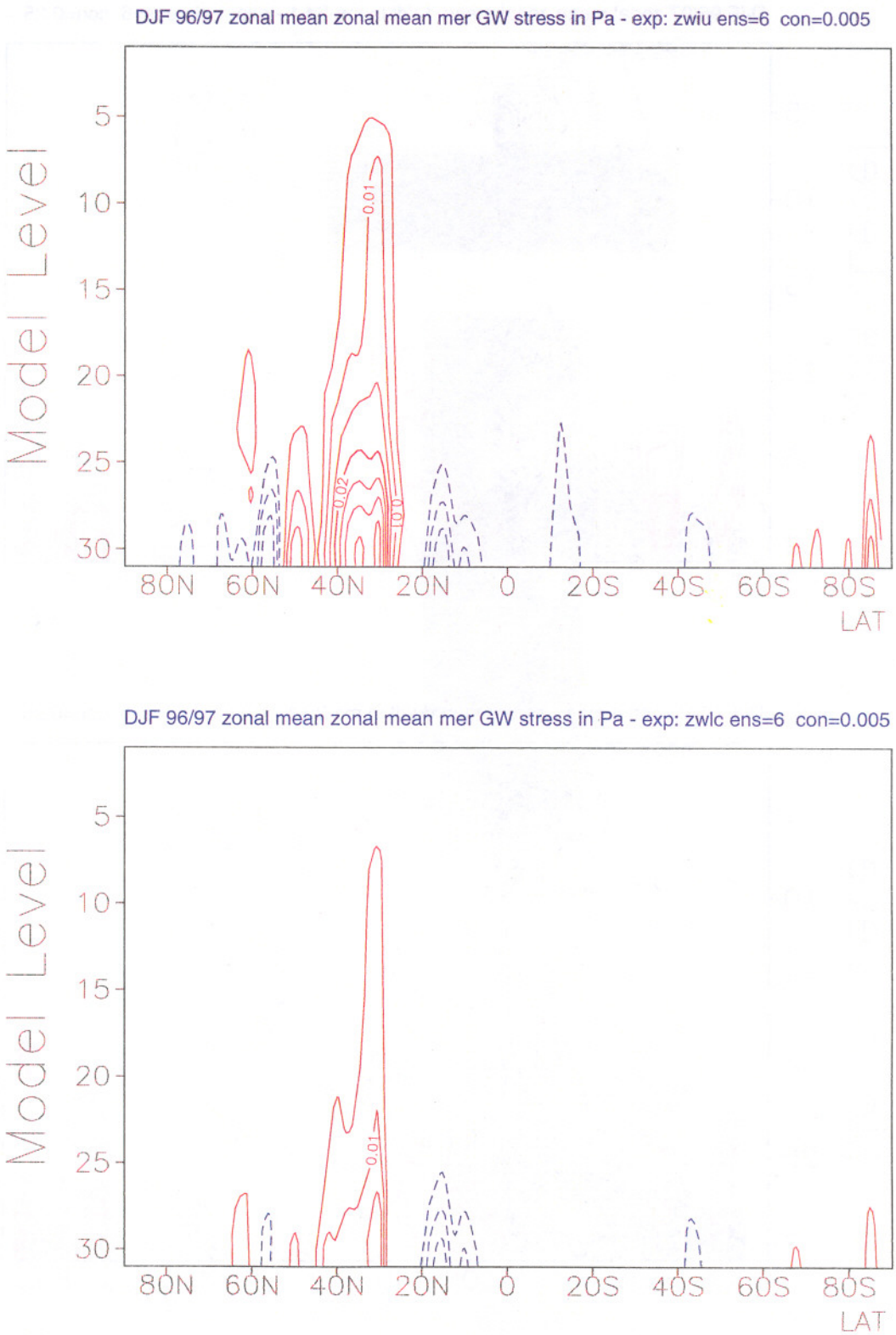

Figure 20: Zonal mean meridional gravity wave stress for (bugcorrected) experiments with new SGO fields (zwiu, top panel), and old fields (zwlc, bottom panel). Contour interval: 0.005 Pa.

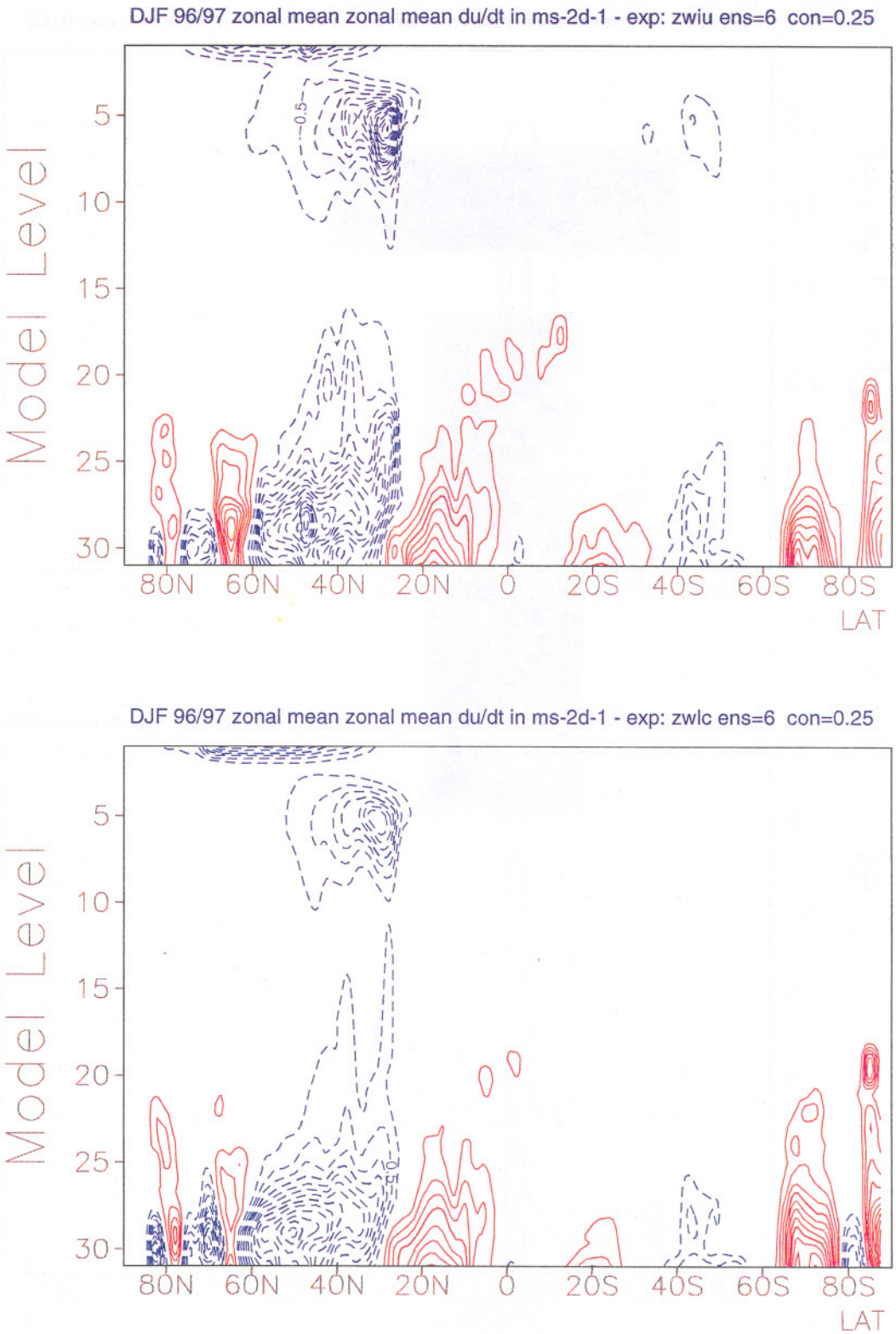

Figure 21: Zonal mean tendency of zonal flow due to SGO scheme for (bugcorrected) experiments with new SGO fields (zwiu, top panel), and old fields (zwlc, bottom panel). Contour interval: 0.25 $ms^{-1}day^{-1}$.

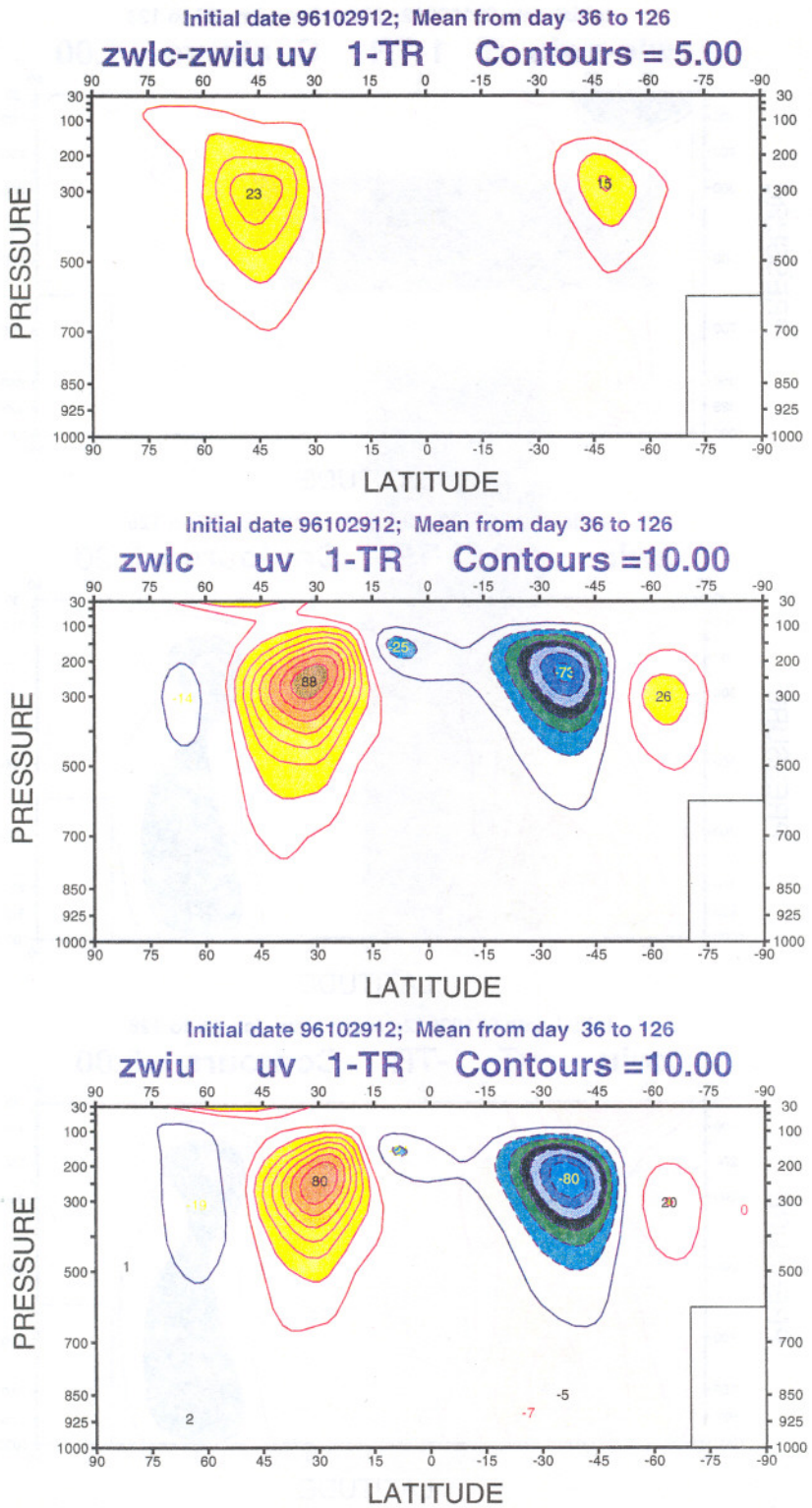

Figure 22: Zonal mean eddy momentum flux for DJF 96/97. Contour interval: 10 m^2s^{-2} for full fields and 5 m^2s^{-2} for the difference. The panels represent: difference between control experiment and experiment with new SGO fields(zwlc-zwiu, top) control experiment with old SGO fields (zwlc, middle), experiment with new SGO fields (zwiu, bottom).

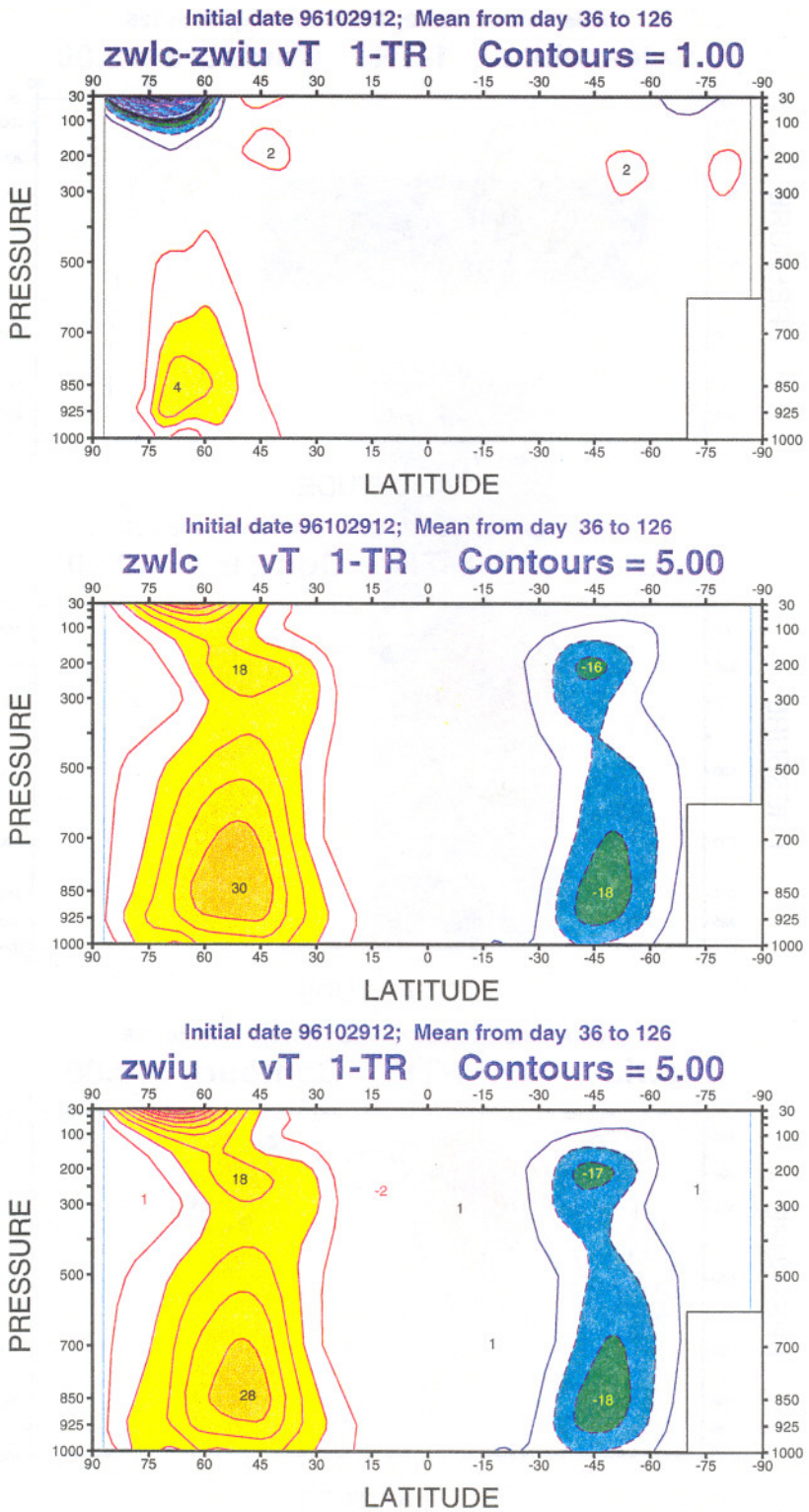

Figure 23: Zonal mean eddy heat flux for DJF 96/97. Contour interval: 5 mKs^{-1} for full fields and 1 mKs^{-1} for the difference. The panels represent: difference between control experiment and experiment with new SGO fields(zwlc-zwiu, top) control experiment with old SGO fields (zwlc, middle), experiment with new SGO fields (zwiu, bottom).

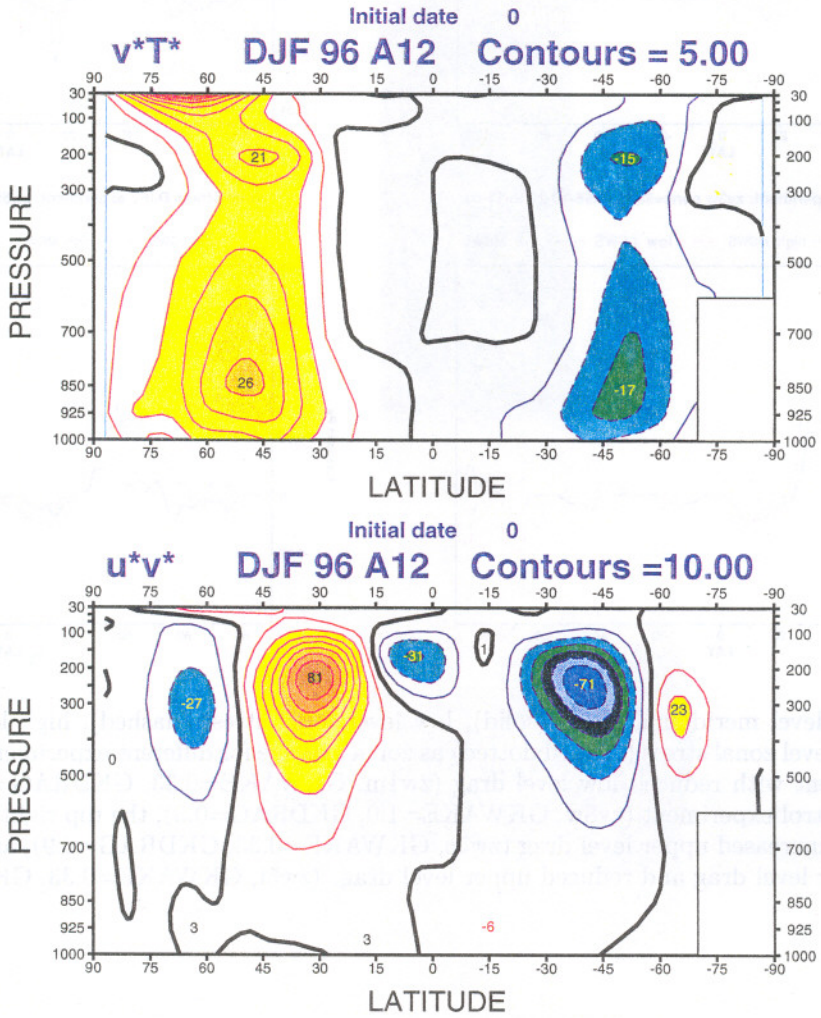

Figure 24: Zonal mean eddy flux from the analysis for DJF 96/97. The panels represent: heat flux (top panel, Contour interval: 5 mKs^{-1}) momentum flux (bottom panel, Contour interval: 10 m^2s^{-2})

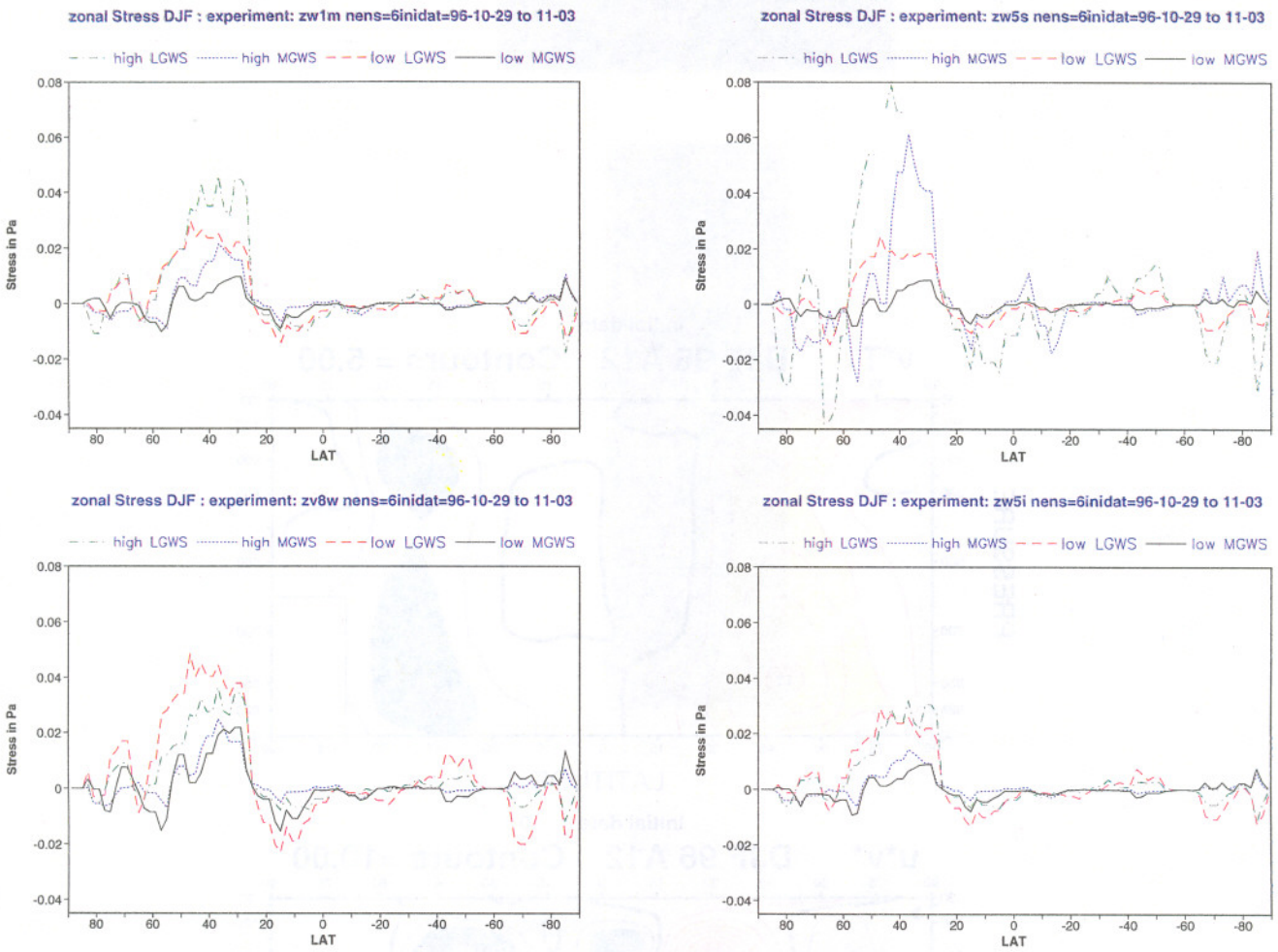

Figure 25: Low level meridional stress (solid), low level zonal stress (dashed), high level meridional stress (dotted) and high level zonal stress (dashed dotted) as zonal average for different experiments. The top left panel is for the experiment with reduced low level drag (zw1m, GKWAKE=0.33, GKDRAG=0.3), the bottom left panel is for the control experiment (zv8w, GKWAKE=1.0, GKDRAG=0.3), the top right panel is with reduced low level drag and increased upper level drag (zw5s, GKWAKE=0.33, GKDRAG=0.9), and bottom right panel is with reduced low level drag and reduced upper level drag. (zw5i, GKWAKE=0.33, GKDRAG=0.2).

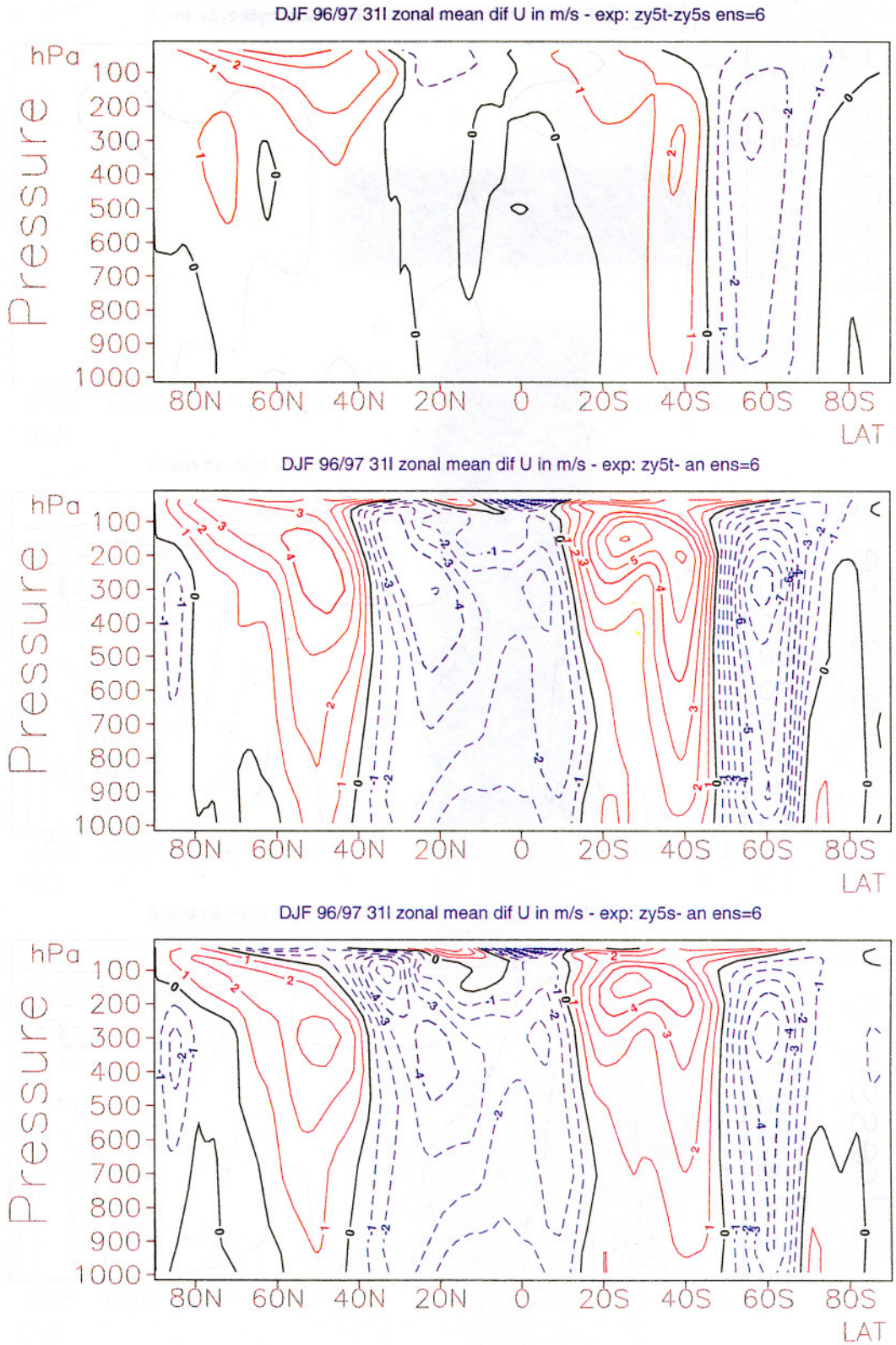

Figure 26: Zonal mean wind difference and errors for DJF 98/99. The top panel represents the difference between the control and the experiment with the new SGO fields (zy5t-zy5s), the middle panel the error of the control experiment (zy5t-ana), and the bottom panel the error of experiment with the new SGO fields (zy5s-ana).

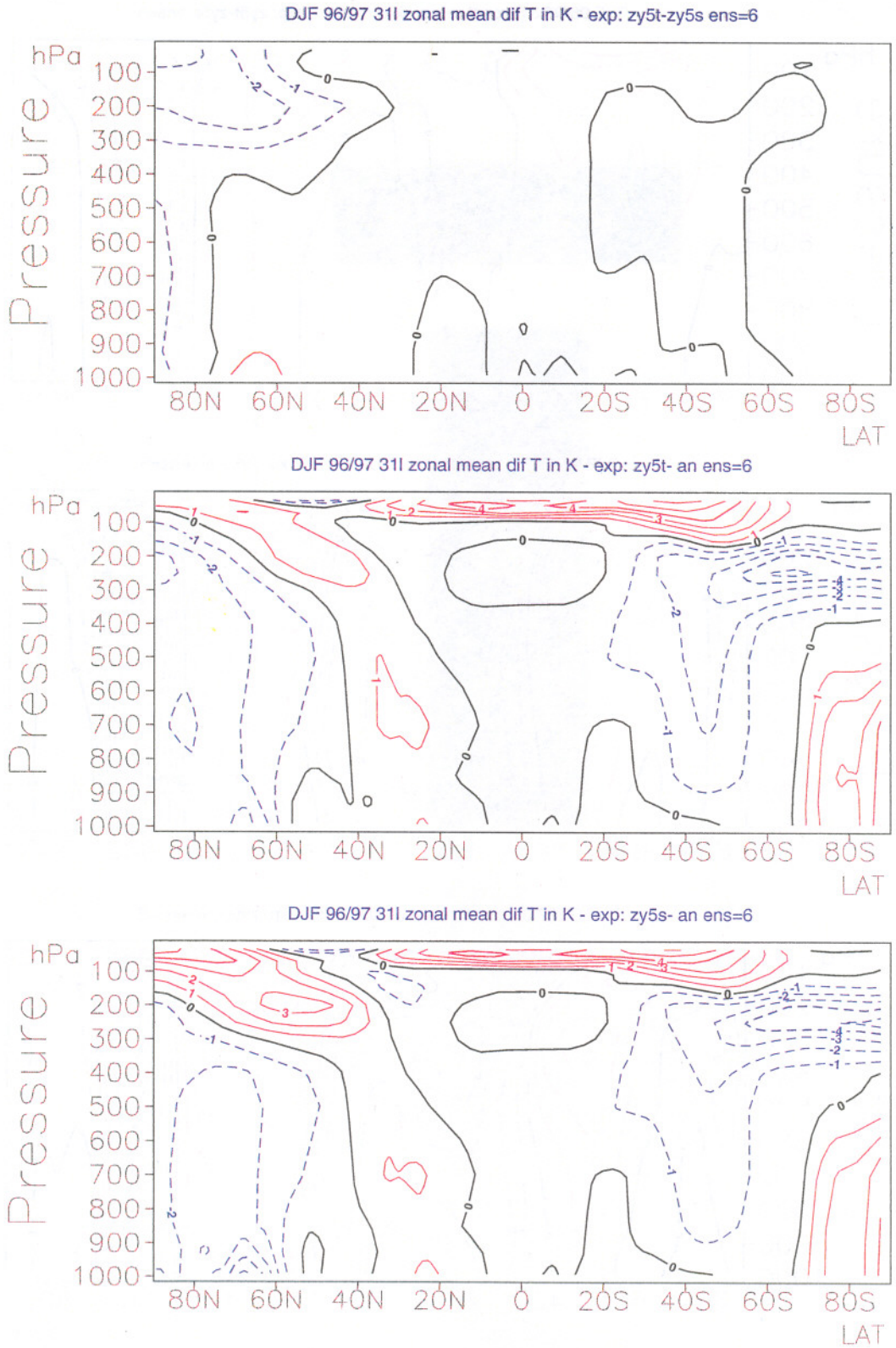

Figure 27: Zonal mean temperature difference and errors for DJF 98/99. The top panel represent the difference between the control and the experiment with the new SGO fields (zy5t-zy5s), the middle panel the error of the control experiment (zy5t-ana), and the bottom panel the error of experiment with the new SGO fields (zy5s-ana).

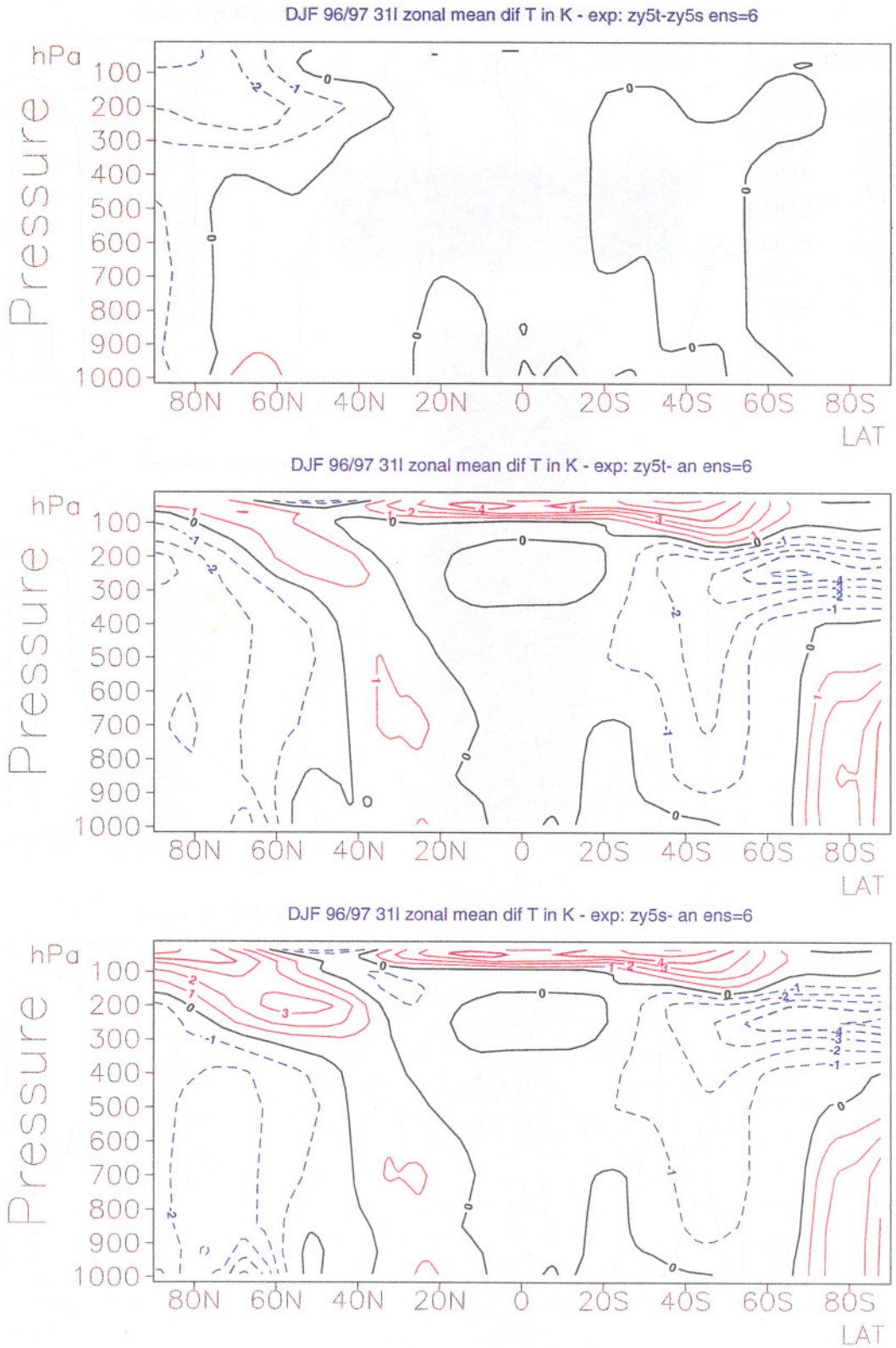

Figure 27: Zonal mean temperature difference and errors for DJF 98/99. The top panel represent the difference between the control and the experiment with the new SGO fields (zy5t-zy5s), the middle panel the error of the control experiment (zy5t-ana), and the bottom panel the error of experiment with the new SGO fields (zy5s-ana).

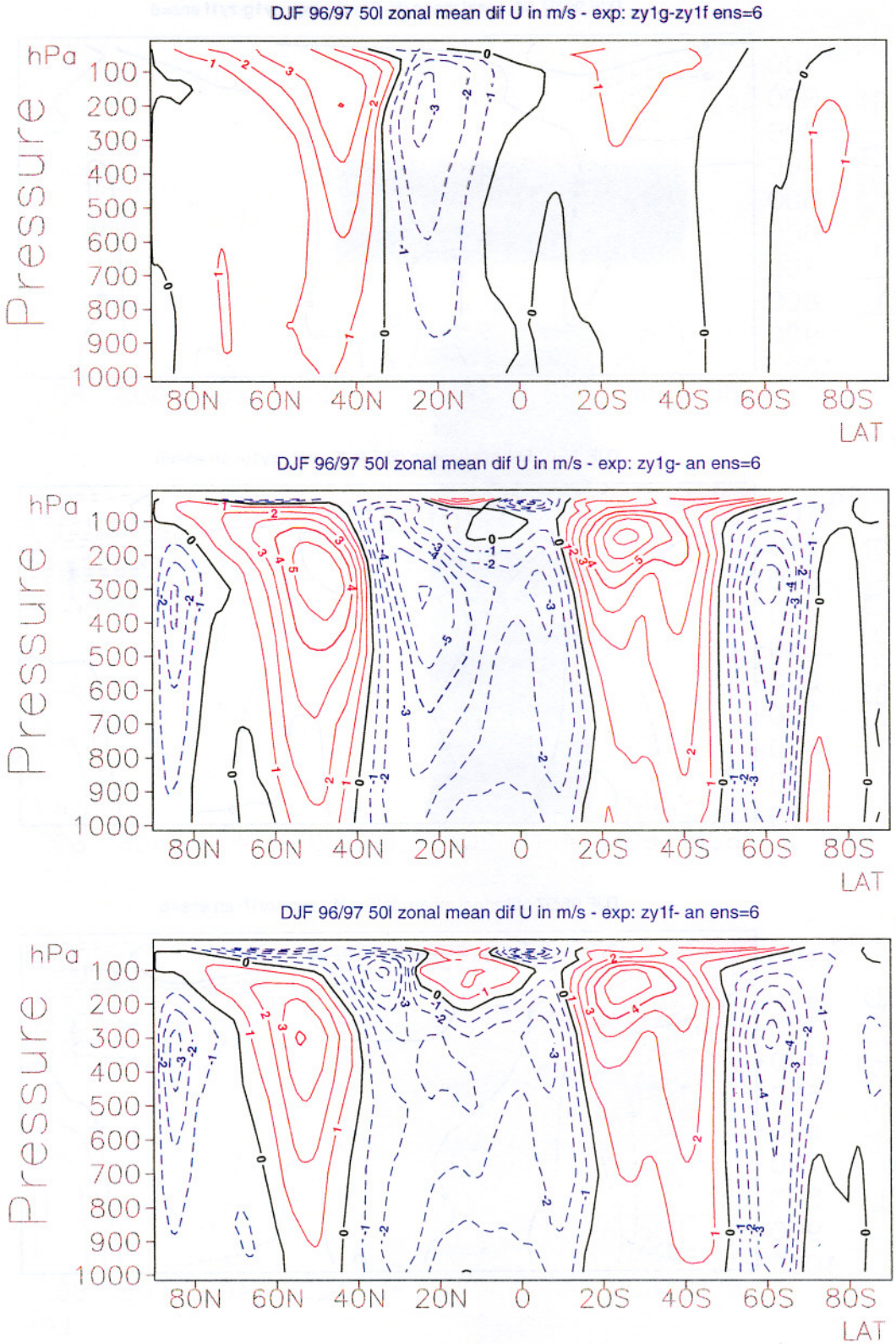

Figure 28: Zonal mean wind difference and errors for DJF 98/99 in the 50 level configuration (model top at 10 Pa instead of 10 hPa as in the 31-level model). The top panel represent the difference between the control and the experiment with the new SGO fields (zy1g-zy1f), the middle panel the error of the control experiment (zy1g-ana), and the bottom panel the error of experiment with the new SGO fields (zy1f-ana).

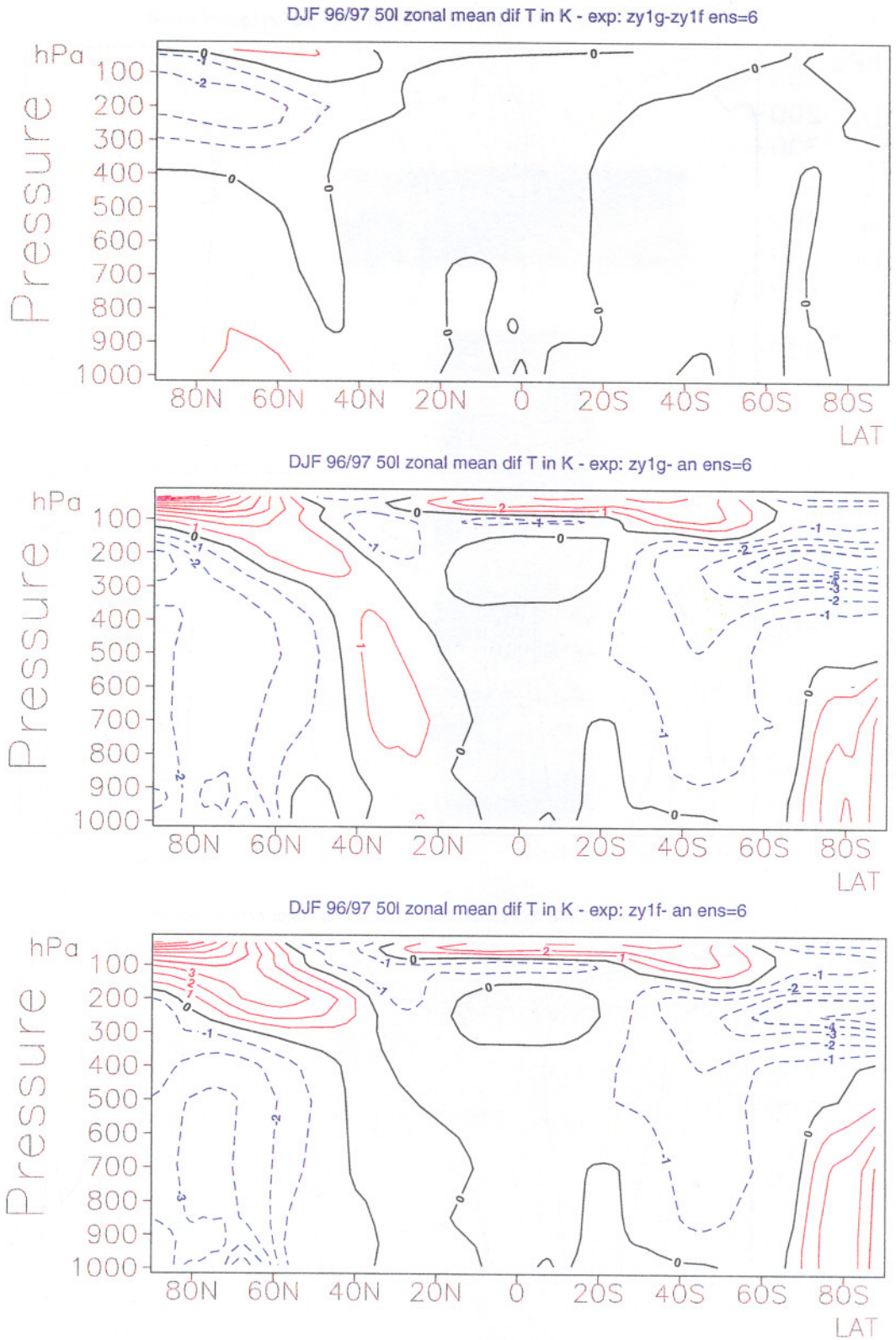

Figure 29: Zonal mean temperature difference and errors for DJF 98/99 in the 50 level configuration (model top at 10 Pa instead of 10 hPa as in the 31-level model). The top panel represent the difference between the control and the experiment with the new SGO fields (zy1g-zy1f), the middle panel the error of the control experiment (zy1g-ana), and the bottom panel the error of experiment with the new SGO fields (zy1f-ana).

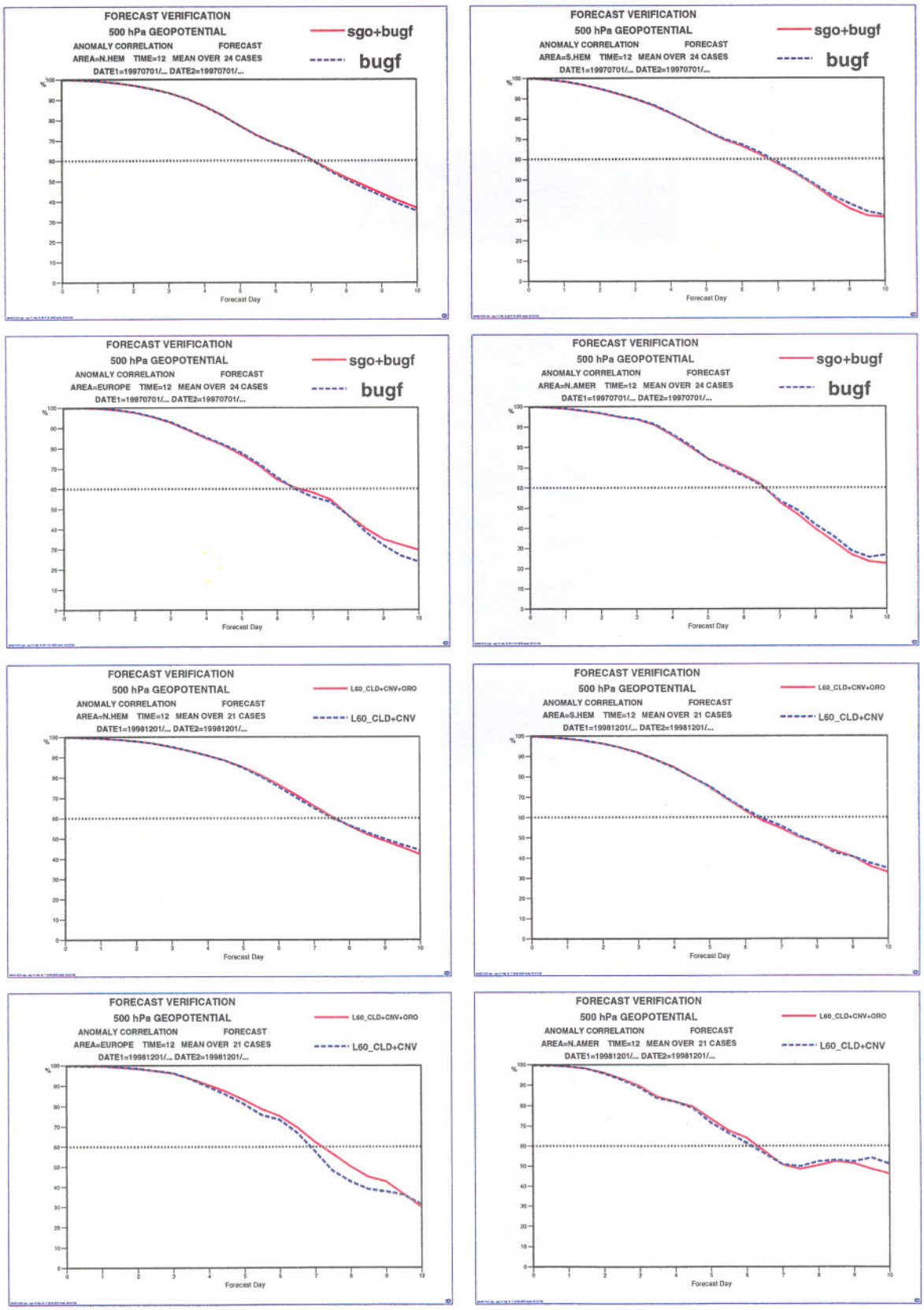

Figure 30: 500 hPa height anomaly correlation for different areas averaged over 24 forecasts spread over an entire year (upper four panels) and for 21 forecasts in January (lower four panels). The solid line is with the new SGO fields and the dashed line is with the old fields.